K-vacancy production in heavy-ion collisions. II. Multiple- and single-collision excitation in the $2p\sigma$ molecular orbital*

W. E. Meyerhof, R. Anholt,† and T. K. Saylor‡
Department of Physics, Stanford University, Stanford, California 94305
(Received 24 January 1977)

The present paper, one of a four-part series, examines K-vacancy cross sections in collisions of symmetric and near-symmetric systems produced with 12–60-MeV Br, 200–330-MeV Kr, 15–80-MeV I, 326–470-MeV Xe, and 90–110-MeV Pb beams. Cross sections are discussed from the point of view of molecular-orbital formation during the collision. In that model, the summed K-vacancy cross sections of both collision partners represents essentially the total $2p\sigma$ vacancy cross section in the outgoing part of the collision. Experimental summed cross sections using solid targets can have appreciable contributions from multiple-collision effects, which are computed in detail. Proposed single-collision mechanisms of $2p\sigma$ vacancy formation are also examined, but none can be established with certainty. The sharing of $2p\sigma$ vacancies on the outgoing part of the collision between the K shells of two collision partners is found to agree well with a previously derived formula based on the Nikitin-Demkov long-range coupling model.

I. INTRODUCTION

The present series of four papers attempts to interpret common features of K-vacancy production cross sections in heavy-ion reactions ($Z \geq 10$). In Ref. 1, henceforth called I, experimental results for projectile (Z_1) and target (Z_2) cross sections were presented. Common trends in the cross sections for a given Z_1 and bombarding energy (E_1) as a function of Z_2 were noted. In the present paper we discuss the cross section features near symmetry, i.e., regions (ii) and (iii) in Figs. 1–6 of I. In order to avoid constant reference to I, we show in Fig. 1 in this paper two sample plots of projectile and target cross sections, which include new data, as well as interpolations and extrapolations from other work.[2-4]

To date innershell vacancy production has been examined theoretically with models using as basis sets either atomic or molecular one-electron wave functions with approximate screening corrections for the other electrons. For brevity we shall call these models "atomic" and "molecular," respectively. Among the former are the plane-wave Born approximation[5] (PWBA), the semiclassical approximation[6] (SCA), and the binary-encounter approximation[7-9] (BEA). Among the latter are the Fano-Lichten promotion model using molecular orbitals[10-14] (MO) and the direct impact ionization theory of Thorson *et al.*[15] The perturbed stationary-state approximation of Basbas *et al.*[16] tries to bridge these approaches, but is applicable only to the excitation of the higher-Z collision partner (see Paper III[17]). The approximate regions of applicability of the various models have been discussed by Madison and Merzbacher.[18] Other reviews are given in Refs. 7 and 19–21.

Roughly speaking, the atomic model and the Basbas model have been most successful for the innershell ionization cross section of the higher-Z partner (usually the target) in very asymmetric collisions. The molecular model has been successfully applied to the innershell vacancy-production cross sections of both collision partners in symmetric or near symmetric collisions for which $v_1/v_e < 1$, where v_1 is the projectile velocity and v_e the velocity of the excited electron, defined by

$$v_e = (2I_e/m)^{1/2} . \tag{1}$$

Here I_e is the (experimental) separated-atom binding energy of the excited electron, and m is the electron mass. Since we are examining K-shell vacancy formation in collisions not far from symmetry, for which $v_1/v_K \lesssim 0.3$, the molecular model should be appropriate. As noted in I, within this model, expressions for the K-vacancy cross sections of the higher-Z (H) and lower-Z (L) collision partners can be obtained by reference to the schematic correlation diagrams sketched in Fig. 2(a) for symmetric and in Fig. 2(b) for asymmetric collisions. (Levels believed not to be relevant to K-vacancy production have been omitted.) From Fig. 2(b) and the discussion in I, one finds

$$\sigma(H) = (1-w)\sigma(1s\sigma) + w\sigma(2p\sigma) , \tag{2}$$

$$\sigma(L) = w\sigma(1s\sigma) + (1-w)\sigma(2p\sigma) + \sigma_{K\text{-}L} . \tag{3}$$

Here $\sigma(1s\sigma)$ and $\sigma(2p\sigma)$ are the cross sections for exciting $1s\sigma$ and $2p\sigma$ vacancies, respectively. According to the model of Ref. 22, both these vacancy cross sections are shared with the same branching ratio $w/(1-w)$. In practice, one finds $\sigma(1s\sigma) \ll \sigma(2p\sigma)$. This can be seen in Fig. 1, where regions (i) represent the $1s\sigma$ excitation cross sec-

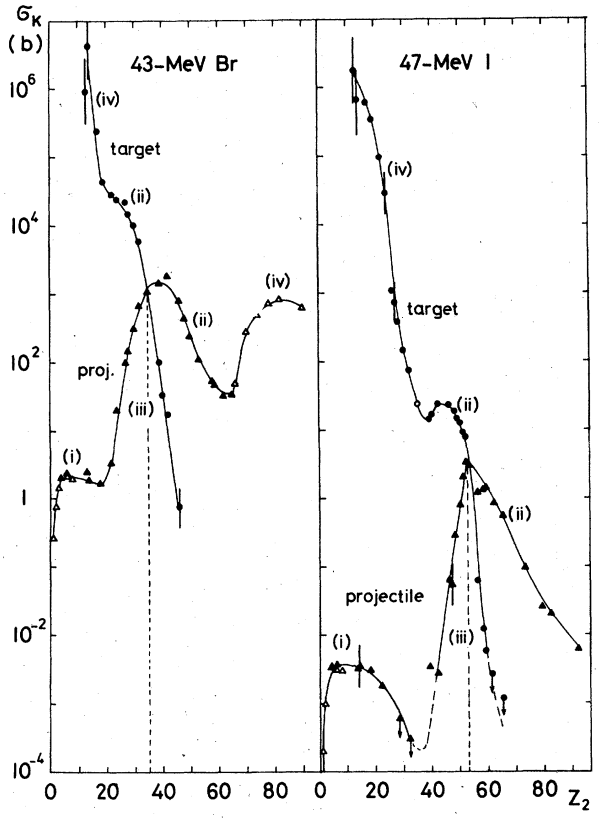

FIG. 1. Projectile and target K-vacancy cross sections for 43-MeV Br and 47-MeV I. Triangles, projectile cross sections; circles, target cross sections. Solid symbols, our work; open symbols, extrapolations or interpolations from other work (Refs. 2–4), including use of inverse collisions (see I). Roman numerals indicate common features in cross sections (see I and text). Dashed vertical lines indicate symmetric collisions. Typical error is ±30%, except where shown.

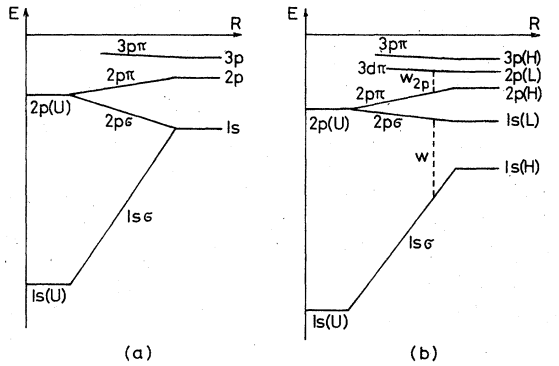

FIG. 2. Schematic correlation diagrams (a) for symmetric and (b) for asymmetric collisions. Only levels relevant to the present discussion are shown. Two vacancy sharing processes w and w_{2p} are indicated in (b). The letters H, L, and U refer to the higher-Z and lower-Z collision partners and to the united atom, respectively.

tions as discussed in Paper III, and regions (ii) the $2p\sigma$ cross sections, as discussed in the present paper. Hence one can determine $\sigma(1s\sigma)$ only if $w \simeq 0$ and use the simplified equations given in I:

$$\sigma(H) = \sigma(1s\sigma) + w\sigma(2p\sigma)\,, \tag{4}$$

$$\sigma(L) = (1-w)\sigma(2p\sigma) + \sigma_{K\text{-}L}\,. \tag{5}$$

The cross section $\sigma_{K\text{-}L}$ arises from K-L level matching effects,[11] when the $1s(L)$ level approaches the $2p(H)$ levels. These effects are discussed in Paper IV. Equations (4) and (5) are no longer valid if the $2p(H)$ and $1s(L)$ levels are close to the swapping point or have swapped.[11] Also, as mentioned in Sec. III, Eqs. (4) and (5) have to be modified if target recoil effects are appreciable.

The present paper concentrates on the cross section $\sigma(2p\sigma)$ and on the vacancy sharing ratio $w/(1-w)$.[12,22-24] By adding Eqs. (2) and (3) or (4) and (5) one finds

$$\sigma(2p\sigma) = \sigma(H) + \sigma(L) - \sigma(1s\sigma) - \sigma_{K\text{-}L}\,. \tag{6}$$

Noting that $\sigma(1s\sigma) \ll \sigma(2p\sigma)$, if the K-L level matching regions [regions (iv) in Fig. 1] are excluded, Eq. (6) reduces to

$$\sigma(2p\sigma) \simeq \sigma(H) + \sigma(L) \equiv \sigma_K^{\text{sum}}\,, \tag{7}$$

i.e., the cross section $\sigma(2p\sigma)$ is given by the experimental summed K-vacancy cross section for both collision partners.

From Eqs. (4) and (5) we also find for the $2p\sigma$ vacancy sharing ratio

$$w/(1-w) = [\sigma(H) - \sigma(1s\sigma)]/[\sigma(L) - \sigma_{K\text{-}L}]\,. \tag{8}$$

Hence only outside of the K-L level matching region and only if we have $\sigma(1s\sigma) \ll \sigma(H)$ can the experimental K-vacancy ratio $\sigma(H)/\sigma(L)$ be compared directly with the calculated ratio $w/(1-w)$. Reference 22 gives the following value for this ratio:

$$w/(1-w) = e^{-2x}\,, \tag{9a}$$

$$2x \equiv \frac{2^{1/2}\pi(I_H^{1/2} - I_L^{1/2})}{m^{1/2}v_1}\,. \tag{9b}$$

Here I_L and I_H are the K-ionization energies of the lower- and higher-Z collision partners, respectively, and v_1 is the projectile velocity. *Ab initio* calculations[12,24] give close agreement with Eqs. (9), for reasons not too well understood.[12]

The experimental summed cross sections [Eq. (7)] are discussed in Sec. II. In Sec. IIA experimental details are given. In Sec. IIB and in Appendix A–D, the effects of multiple collisions in solid targets in relation to Eq. (7) are examined carefully. In regions of Z_1, Z_2 near symmetry these effects turn out to be very large. In Sec. IIC the single-collision $2p\sigma$ cross section is compared to present theoretical proposals involving

ionization or electron promotion. In Sec. III the K-vacancy sharing ratio (8) is discussed and possible limitations to Eqs. (9a) and (9b) are explored.

II. SUMMED K-VACANCY CROSS SECTIONS

A. Experimental

As described in I, most of our measurements were made with thick solid targets. Cross sections were extracted from thick-target yields by the Merzbacher-Lewis formula,[5] since recoil effects[25,26] were shown to be of the order of one percent or less, which is negligible compared to a typical experimental error of ±30%.

Figure 3 shows the summed K-vacancy cross section (a) for $_{35}$Br and $_{36}$Kr projectiles and (b) for $_{53}$I and $_{54}$Xe projectiles, as a function of target Z. The projectile energies in MeV are given adjacent to the curves drawn to guide the eye. Some data is taken from Refs. 2 and 27. For Br and Kr dramatic increases in the cross section occur for $Z_2 \lesssim 20$ and $Z_2 \gtrsim 65$. These are due to K-L level matching effects,[28] which form the subject of Paper IV and which are not discussed further here. For I and Xe the K-L level matching effect appears for $Z_2 \lesssim 30$.

In Figs. 3(a) and 3(b) slight humps can be seen in the cross-section trends near symmetry, especially at the lower bombarding energies. We show in Sec. II B that, most likely, these humps are due to multiple collision effects[29-31] in solid targets.

The bombarding energy dependence of σ_K^{sum} is illustrated in Fig. 4 for symmetric collisions with $Z_1 = Z_2 \geq 10$. Gas and solid target data are taken from our and other work.[2,26,27,32-40] Some individual cross sections have been interpolated from the crossover of the target and projectile cross sections at symmetry (e.g., see Fig. 1). If only x-ray cross sections were determined, they have been converted to vacancy cross sections using the fluorescence yields of Ref. 59. The bombarding energy dependence of asymmetric summed cross sections is similar to that shown in Fig. 4.

B. Multiple-collision effects

1. *Thick targets: Theory*

For collisions with $Z_1, Z_2 \leq 10$, it has been demonstrated by many experiments that the Fano-

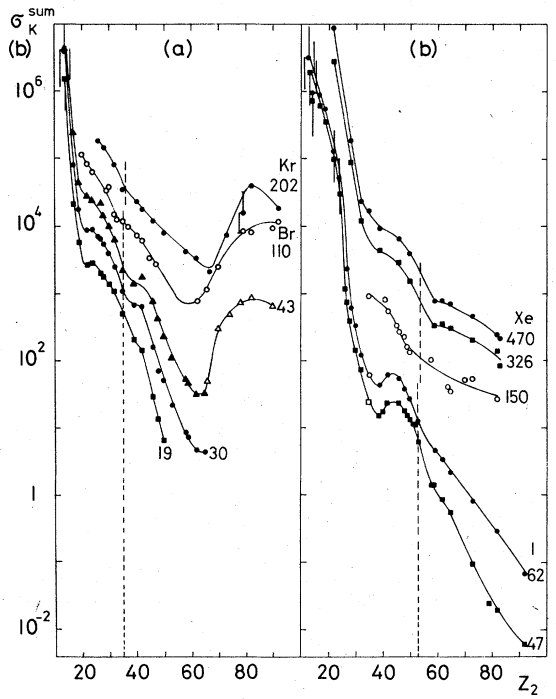

FIG. 3. Summed K-vacancy cross sections for both collision partners as a function of target atomic number (a) for Br and Kr projectiles and (b) for I and Xe projectiles. Numbers give projectile energies in MeV. Closed symbols, our work; open symbols, other work (Refs. 2 and 27). Vertical dashed lines indicate symmetric collisions. Thin solid lines are only to guide the eye. Typical errors are ±30%, except where shown.

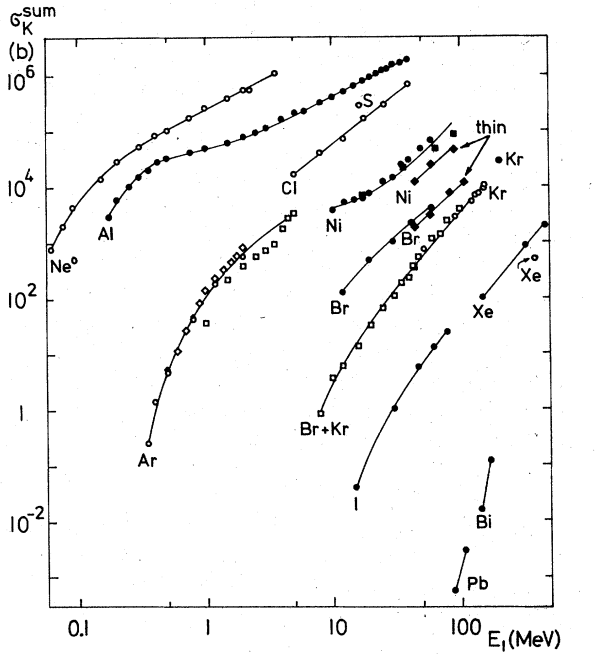

FIG. 4. Summed K-vacancy cross sections for symmetric collisions as a function of bombarding energy. Open symbols, gas targets; closed symbols, solid targets. Typical errors are ±10 to 30 percent. Data from the following references: Ne^0 (neutral Ne), Ref. 32; Al, Refs. 26 and 33, S, Cl, Ref. 34; Ar, ○, Ref. 35; □, Ref. 36; ◇, Ref. 37; Ni, ●, Ref. 33; ■, Ref. 56; ♦, Ref. 2 (thin target); Br, ●, present work; ♦, Ref. 2 (thin target); Br+Kr, □, Ref. 40; Kr, present work; I and Xe, present work; Pb, Ref. 39; Bi, Ref. 38.

Lichten $2p\sigma$-$2p\pi$ electron promotion process dominates $2p\sigma$ vacancy formation.[20,21] For $Z_1, Z_2 \geq 10$, the $2p\pi$ MO is generally filled. Nevertheless, electron promotion could operate by means either of a *one-collision* two-step process or by a *multiple-collision* process. In the one-collision two-step process, the filled $2p\pi$ MO could couple to vacant projectile or target states, e.g., via the $3p\pi$ MO shown in Fig. 2; the resulting $2p\pi$ vacancies could be filled by $2p\sigma$-$2p\pi$ electron promotion.[21] This process, as well as a proposed one-collision one-step process of $2p\sigma$ vacancy formation are examined in Sec. IIC. Hence it is useful to rewrite Eq. (7) as

$$\sigma_K^{\rm sum} = \sigma(2p\sigma) = \sigma_{\rm sc}(2p\sigma) + \sigma_{\rm mc}(2p\sigma)\,, \tag{10}$$

where the subscripts sc and mc denote single- and multiple-collision processes, respectively. Here we concentrate on the latter.

The multiple-collision process is due to projectile $2p$ vacancies, made in some collision, which live long enough to be carried into a second collision, where $2p\sigma$-$2p\pi$ promotion can operate. If target recoil processes[25,26] are negligible, only the projectile can move from one target atom to the next and, hence, only projectile $2p$ vacancies need to be considered. Multiple-collision effects are important in solid targets, because the repeated excitation of projectile electrons produces an appreciable steady-state vacancy distribution among the projectile inner shells. In gas targets there will also be a steady-state distribution of vacancies, but the fraction of vacancies in the K and L shells is generally negligibly small.

It has been shown by Lennard and Mitchell[41] that if a projectile carries $2p$ vacancies into a collision these vacancies are shared between the $2p\pi$ and $3d\pi$ MO's in a ratio analogous to Eq. (9a) [see Fig. 2(b)]. Combining this with Eq. (5) of Ref. 14, the multiple-collision contribution to $\sigma(2p\sigma)$ due to steady-state projectile $2p$ vacancies is found to be[41]

$$\sigma_{\rm mc}(2p\sigma, v) = \tfrac{1}{3} n(v) w_{2p} \sigma_{\rm rot}\,. \tag{11}$$

Here $n(v)$ is the total number of $2p$ vacancies carried by the projectiles moving with velocity v inside the target material divided by the number of projectiles:

$$n(v) = \sum_{k=1}^{6} k f_k(v)\,, \tag{12}$$

where $f_k(v)$ is the fraction of projectiles carrying k vacancies. (Here, we do not distinguish between $2p_{1/2}$ and $2p_{3/2}$ vacancies; see Appendix C.) The cross section $\sigma_{\rm rot}$ is the $2p\sigma$-$2p\pi$ rotational coupling cross section per incident $2p\pi_x$ vacancy,[13,42] the factor $\frac{1}{3}$ is a statistical factor derived by Macek and Briggs[14] and the $2p$-vacancy sharing fraction w_{2p} is given by an equation similar to Eq. (9a):

$$w_{2p} = (1 + e^{2x'})^{-1}\,, \tag{13}$$

$$2x' = 0.89 \frac{2^{1/2}\pi (I_2^{1/2} - I_1^{1/2})}{m^{1/2} v}\,, \tag{14}$$

where I_1 and I_2 are the $2p$ ionization energies of the projectile and target atoms, respectively. The factor 0.89 in Eq. (14) has been determined empirically.[41] If the projectile is the higher-Z partner, $x' \to -x'$ and $w_{2p} \to 1 - w_{2p}$, so that Eqs. (11)–(13) are applicable for $Z_1 > Z_2$, as well as for $Z_1 \leq Z_2$.

For a thick target, expression (11) has to be integrated over the projectile path. We have extended a formulation developed by Garcia and Fortner,[43,44] in order to separate the single- and multiple-collision contributions to the thick-target yield and in order to include the possibility of projectile $2p$-vacancy quenching,[45,46] as well as $2p$-vacancy decay. From Ref. 44 one finds that the projectile vacancy fraction f_k in Eq. (12) is of order $(f_1)^k$, if $f_1 \ll 1$. With this assumption, which implies $n(v) \simeq f_1(v)$, Garcia[43] develops a relation between cross-section and thick-target yield. Generalizing this relation, we show in Appendix A that to a high degree of accuracy the following equation holds at the *incident* projectile velocity v_1:

$$\sigma_K^{\rm sum}(ML, v_1) = \sigma_{\rm sc}(2p\sigma, v_1) + \sigma_{\rm mc}^{(1)}(2p\sigma, v_1)\,, \tag{15}$$

as suggested in Eq. (10). Here $\sigma_K^{\rm sum}(ML, v_1)$ is the summed target and projectile K-vacancy cross section extracted from the thick-target yields by the Merzbacher-Lewis formula.[5] In Eq. (15) the multiple collision cross section due to the vacancy fraction f_1 is found to be [Eqs. (A8), (A17), (A18)]

$$\sigma_{\rm mc}^{(1)}(2p\sigma, v_1) = \tfrac{1}{3} f_1^{\rm eq}(v_1) w_{2p} \sigma_{\rm rot}\,, \tag{16}$$

where $f_1^{\rm eq}$ is the equilibrium value of the steady-state projectile fraction carrying one $2p$ vacancy.[45-47] Therefore, to a high degree of accuracy (in our case, approximately 1%) the thick-target expression for $\sigma_{\rm mc}^{(1)}$ is identical to the thin-target expression (11), applied to a thin target of sufficient thickness so that the steady-state projectile $2p$-vacancy fraction has reached its equilibrium value.[45,46] Because the complete system of rate equations for $f_k(v)$ is difficult to solve,[44] we assume, as seems reasonable, that for the other vacancy fractions f_k with $k > 1$, a thin-target expression analogous to Eq. (16) will also be valid for a thick target:

$$\sigma_{\rm mc}^{(k)}(2p\sigma, v_1) = \tfrac{1}{3} k f_k^{\rm eq}(v_1) w_{2p} \sigma_{\rm rot}\,.$$

Adding the contributions from all the vacancy fractions, and using Eq. (12), we then arrive at the final expression

$$\sigma_{mc}(2p\sigma, v_1) = \tfrac{1}{3} n^{eq}(v_1) w_{2p} \sigma_{rot} , \quad (17)$$

where $n^{eq}(v_1)$ is the equilibrium value of the steady-state $2p$-vacancy number per projectile [Eq. (12)]. Correspondingly, Eq. (15) is changed to

$$\sigma_K^{sum}(ML, v_1) = \sigma_{sc}(2p\sigma, v_1) + \sigma_{mc}(2p\sigma, v_1) . \quad (18)$$

In Appendix B we show that the value of $f_1^{eq}(v_1)$ in Eq. (16) can be obtained *experimentally* from the projectile $2p(L_2+L_3)$ *x-ray* cross section $\sigma_{proj\,x}^{2p(1)}(ML, v_1)$ extracted from the thick-target yield by the Merzbacher-Lewis formula.[5] Again quenching, as well as decay, of projectile $2p$ vacancies is included and, again, the assumption $f_k(k>1) \ll f_1$ is made. Under these conditions, the relation between $\sigma_{proj\,x}^{2p(1)}(ML, v_1)$ and $f_1^{eq}(v_1)$ for an elemental target of atomic density n_2 is [Eq. (B9), but observe slightly different notation]:

$$n_2 v_1 \sigma_{proj\,x}^{2p(1)}(ML, v_1) = f_1^{eq}(v_1)/\tau_{1x} , \quad (19)$$

where τ_{1x}^{-1} is the decay constant for x-ray emission from a projectile with one $2p$ vacancy. This equation is very similar to the thin-foil expression in Ref. 45, assuming all the yield comes from inside the foil. Assuming again that equations similar to (19) exist for the contributions from the other vacancy fractions f_k, one obtains for the total projectile $2p$ x-ray cross section:

$$n_2 v_1 \sigma_{proj\,x}^{2p}(ML, v_1) = \sum_{k=1}^{6} \frac{f_k^{eq}(v_1)}{\tau_{kx}} , \quad (20)$$

where τ_{kx}^{-1} is the decay constant for (single) photon emission from a projectile with k $2p$ vacancies. This equation is consistent with Eq. (1) of Ref. 44. Now we assume that the radiative decay constant of a projectile with k $2p$ vacancies is approximately equal to k times the radiative decay constant of a projectile with a single $2p$ vacancy, an approximation similar to one made in Ref. 47:

$$\tau_{kx}^{-1} \simeq k \tau_{1x}^{-1} .$$

Substitution into Eq. (20) then yields, using Eq. (12),

$$n^{eq}(v_1) = n_2 v_1 \tau_{1x} \sigma_{proj\,x}^{2p}(ML, v_1) . \quad (21)$$

For a compound target one needs only to replace $n_2 \sigma_{proj\,x}^{2p}$ by expression (B8). Equation (21) can be substituted into Eq. (17) to obtain the multiple-collision cross section $\sigma_{mc}(2p\sigma, v_1)$ in Eq. (18) in terms of known quantities:

$$\sigma_{mc}(2p\sigma, v_1) = \tfrac{1}{3} n_2 v_1 \tau_{1x} \sigma_{proj\,x}^{2p}(ML, v_1) w_{2p} \sigma_{rot} . \quad (22)$$

We wish to stress the generality of Eqs. (17), (21), and (22). In particular we emphasize that $2p$-vacancy quenching is taken fully into account. The $2p$-vacancy number per projectile $n^{eq}(v_1)$ is determined experimentally from the $2p$ x-ray cross section and not from expressions for the production, quenching, and decay mean free paths,[45] essentially by combining Eqs. (A18) and (B6). In Appendix C we also show that, with relatively minor assumptions, the Coster-Kronig transitions from the L_1 to the L_2 and L_3 subshells and between the L_2 and L_3 subshells do not affect Eq. (19), nor, presumably, Eq. (21).

In Sec. II B 2 we apply Eqs. (17), (21), and (22). Therefore, the determinations of τ_{1x} and of σ_{rot} need some discussion. Since the main contributions to τ_{1x}^{-1} arise from electronic transitions originating in the $M4$ and $M5$ subshells,[48] one would expect that stripping of projectile M electrons in the solid target should have a major effect on τ_{1x}^{-1}. Nevertheless, Kauffman *et al.*[49] have found the effective number of M electrons in 45-MeV Cl projectiles traversing solid Si to be much higher than simple stripping ideas would lead one to suspect. Therefore, tentatively, we have used tabulated single-$2p$-vacancy values for τ_{1x}^{-1} in Eq. (21), for Br and I projectiles. By comparing $n^{eq}(v_1)$ from Eq. (21) with $n^{eq}(v_1)$ computed from Eq. (17) we can check *experimentally* whether our tentative values for τ_{1x}^{-1} are reasonable (see Sec. II B 2).

For σ_{rot} in Eqs. (17) and (22) we have used the scaling procedure of Taulbjerg *et al.*[42] But, since in some of our collision systems the united-atom atomic number exceeds 100, we felt it necessary to investigate the possible effect on σ_{rot} of spin-orbit splitting at small internuclear separations.[50] We found that for 19–43-MeV Br collisions the spin-orbit effect is only minor, but that for 15–62-MeV I collisions the spin-orbit effect can decrease σ_{rot} appreciably. An approximate spin-orbit correction factor is obtained in Ref. 50, which could be applied to σ_{rot} computed from Ref. 42.

2. *Thick targets: Experiment*

We now apply Eqs. (17) and (21) in two different ways. First, using Br projectiles on solid KBr and I projectiles on solid NaI targets we compare the values of $n^{eq}(v_1)$ obtained from Eq. (17) with those computed from Eq. (21). For this purpose we had to determine $\sigma_{mc}(2p\sigma, v_1)$ from experiment through the use of Eq. (18). Second, by eliminating $n^{eq}(v_1)$ between Eqs. (17) and (21) to obtain Eq. (22), we compute the multiple collision contributions to the Br and I summed K-vacancy cross sections shown in Fig. 3.

For reference we show in Fig. 5 our measurements of total projectile L x-ray cross sections with Br and I beams as a function of target Z. Also shown are the sparse cross sections measured elsewhere.[2,31,51-54] In the case of I agree-

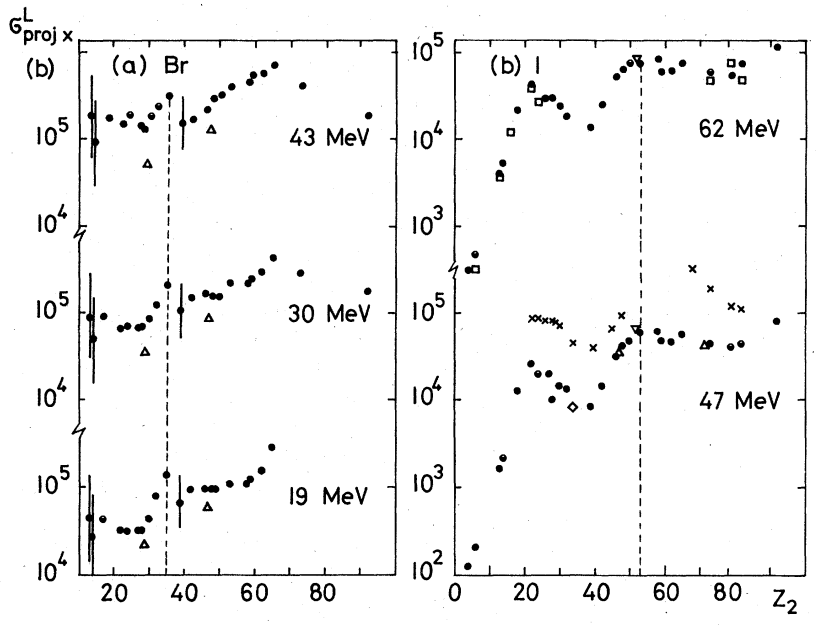

FIG. 5. Projectile L x-ray cross sections (a) for Br and (b) for I beams as a function of target atomic number. Typical error ±30%, except where shown. In (a), △, Ref. 54 (thin target). In (b), □, Ref. 51 (60 MeV); ◇, Ref. 31 (48 MeV); △, Ref. 2 (50 MeV); ▽, Ref. 52 (one-half of the total I+Te L x-ray cross section); ×, Ref. 53 [L x-ray cross section of 42-MeV heavy fission products for which $Z_1(\mathrm{av}) \simeq 54$]. Vertical dashed lines indicate symmetric collisions.

ment is satisfactory to within the ±30% error we assign to our cross sections.[1] In the case of Br there exists the possibility of multiple-collision thin-target effects in the work of Ref. 54, which may influence the Merzbacher-Lewis L x-ray cross section, as they do the K cross section (see Sec. IIB3). To obtain the $2p$ x-ray section needed in Eqs. (21) and (22) from the total L x-ray cross section, we multiplied the latter by 0.9,[2,55] which is a minor correction compared to the error on the cross sections.

Figures 6(a) and 6(b) give comparisons of $n^{eq}(v_1)$ extracted from Eq. (17) (data points) with those calculated from Eq. (21) (lines), for Br+Br and I+I collisions, respectively. To obtain $\sigma_{mc}(2p\sigma, v_1)$ we assumed that in Eq. (18) the *single-collision* cross section $\sigma_{sc}(2p\sigma, v_1)$ in a solid target is equal to the single-collision cross section in a gas target, which should be reasonable for innershell excitations. For Br+Br, we used the Br+Kr and Kr+Kr gas-target cross sections shown in Fig. 4. For I+I we used the gas-target scaled cross section plot of Fig. 10(a) discussed in Sec. IIC (note that a measured point for Xe+Xe lies on this plot). Figure 4 shows that at the lower bombarding energies the single-collision contribution to σ_K^{sum} in a solid is small.

In Fig. 6(a), a thin-target correction, discussed in Sec. IIIB3, was applied to $\sigma_{mc}(2p\sigma, v_1)$ for the Br+Br data obtained from Ref. 2. In Fig. 6(b), we show the data points for $n^{eq}(v_1)$ without and with the correction for spin-orbit effect on σ_{rot}.[50] We suspect that at low bombarding energies the spin-orbit correction factor for σ_{rot} is too large, making the $n^{eq}(v_1)$ values computed from Eq. (17) too small.[50]

It turns out that Eq. (21) can be represented by a straight line on a log-log plot, because over the limited range of energies used here the L x-ray cross section has a power law dependence on E_1 (compare Refs. 52 and 54). Of course a ±30% error is attached to the lines shown in Figs. 6(a) and 6(b). The agreement between the two ways to obtain $n^{eq}(v_1)$ is satisfactory and indicates the basic correctness of Eqs. (17) and (21), as well as the apparent validity of using for τ_{1x}^{-1} the single $2p$-vacancy values of Ref. 48. This must indicate an appreciable presence of M electrons in Br and I projectiles in solids, similar to the findings of Ref. 49 for Cl.

In Fig. 6(c) we present an independent check of Eq. (17) using Ni+Ni cross-section measurements of Refs. 33 and 56. To obtain $\sigma_{mc}(2p\sigma, v_1)$ we again use Eq. (18) and estimate $\sigma_{sc}(2p\sigma, v_1)$ from Fig. 10(a). The values of $n^{eq}(v_1)$ so obtained from Eq. (17) are shown by the data points in Fig. 6(c) which reflect an inconsistency in the cross section measurements of Refs. 33 and 56 at higher bombarding energies. Here, projectile L x-ray cross sections were not determined, but an estimate of the average number of L-shell vacancies per projectile was made in Ref. 33 from the $K\alpha$ x-ray energy shift. This estimate is represented in Fig. 6(b) by the straight line and its associated error. Taking into account the possible contribution of $2s$ vacancies to the average $K\alpha$ x-ray energy shift, there is reasonable agreement with the values of $n^{eq}(v_1)$ computed from Eq. (17).

Figure 6 gives us confidence that Eq. (22) should yield the correct multiple collision contribution

$\sigma_{mc}(2p\sigma)$ to the σ_K^{sum} plots of Fig. 3, some of which are repeated in Figs. 7 and 8. Using the L x-ray cross sections from Fig. 5, Eq. (22) yields the curves shown in Figs. 7 and 8. The solid lines assume no spin-orbit effect on σ_{rot}, the dashed lines use the correction factor of Ref. 50. For sake of clarity, individual points have been omitted and smooth curves have been drawn through them. Because of uncertainties in the measured L x-ray cross sections, a ±30% error is attached to these curves, along the ordinate. One can see that in a fairly wide-Z_2 region near symmetry, σ_K^{sum} appears to be dominated by multiple-collision effects. Also one can see that the peculiar humps in σ_K^{sum}, noted in Fig. 3, reflect the behavior of $\sigma_{mc}(2p\sigma)$, which in turn reflects level matching effects in the projectile L x-ray cross section[53] (Fig. 5), as well as the strong-Z_2 dependence of w_{2p} [Eqs. (13) and (14)] for $Z_2 > Z_1$.

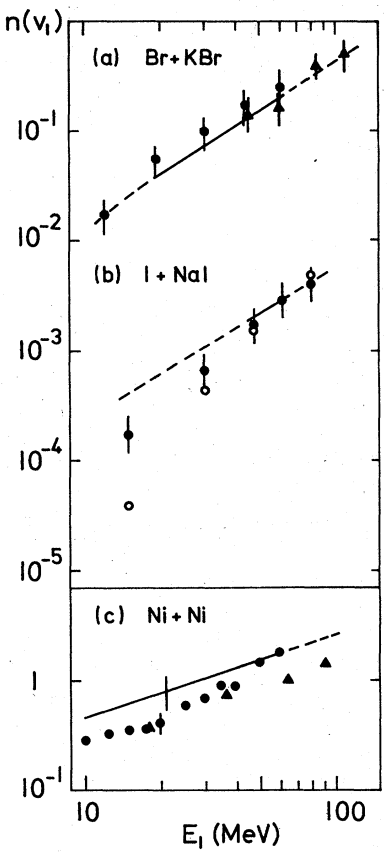

FIG. 6. Equilibrium number of projectile $2p$ vacancies (a) in Br+KBr collisions, (b) in I+NaI collisions, and (c) in Ni+Ni collisions. Experimental points extracted with the use of Eqs. (17), (18) and (25). (a) Data: ●, from present work, using Eq. (17); ▲, from Ref. 2, using Eqs. (25) and (17). Line: Eq. (21), using data from Fig. 5(a) and Ref. 54. (b) Data: from present work, ○, not corrected; ●, corrected for spin-orbit effect on σ_{rot}. Line: Eq. (21), using data from Fig. 5(b) and Ref. 52. (c) Data: ●, Ref. 33; ▲, Ref. 56, using Eq. (17). Line represents total L vacancy number per projectile estimated in Ref. 33 from K_α energy shift. Typical errors are shown.

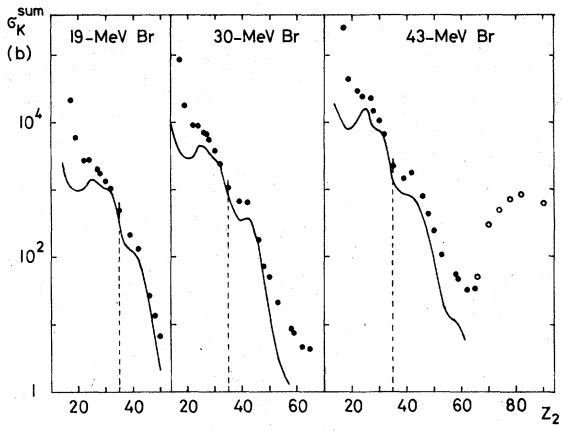

FIG. 7. Summed K-vacancy cross sections for Br as a function of target Z. Curves represent computed multiple-collision contribution to $2p\sigma$ cross section [Eq. (22)]. Spin-orbit effect on σ_{rot} lowers curves by less than 20% at highest Z_2 values. Errors on data and on computed curves are ±30%, each. Vertical dashed lines indicate symmetry. At low and high values of Z_2, K-L level matching effect is apparent in the data.

The computed curves for $\sigma_{mc}(2p\sigma)$ could be affected by a variety of effects which we have not included, such as vacancy transfer to the $2p\pi$ MO from higher MO's than the $3d\pi$ MO and changes in the values of I_1 in Eq. (14) due to projectile ionization in the target material. These effects would

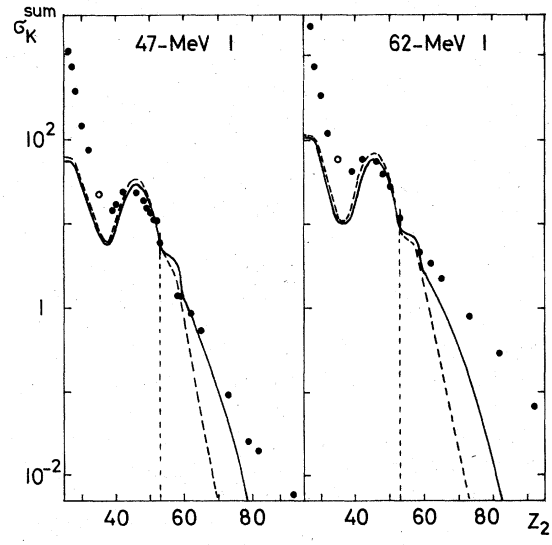

FIG. 8. Summed K-vacancy cross sections for I as a function of target Z. Same caption as for Fig. 7, except that spin-orbit effect on σ_{rot} is included in dashed curves.

tend to increase $\sigma_{mc}(2p\sigma, v_1)$. It is also possible that the scaling relations of Ref. 42 are not valid at large asymmetry.[41] Nevertheless, we feel that the overall agreement of $\sigma_{mc}(2p\sigma, v_1)$ with σ_K^{sum} in regions (ii) of Fig. 1 supports our interpretation of these cross sections.

3. *Thin targets*

If the formalism of Appendixes A–C is applied to sufficiently thin targets, the energy variation of the beam within the target foil can be neglected.[45,57] In Appendix D we consider a target foil of atomic density n_2 and of thickness t traversed by the beam. If the foil is mounted on a backing of thickness b, such that the beam first traverses the backing, Eq. (18) is replaced by

$$\sigma_K^{sum}(\text{thin}) = \sigma_{sc}(2p\sigma, v_1) + \sigma_{mc}(2p\sigma, \text{thin}) , \tag{23}$$

where

$$\sigma_K^{sum}(\text{thin}) = Y/n_2 t \tag{24}$$

and

$$\sigma_{mc}(2p\sigma, \text{thin}) = \sigma_{mc}(2p\sigma, \text{thick}) \times\left[1-\left(1-\frac{n^b(v_1)}{n^{eq}(v_1)}\right)\frac{1-\exp(-\sigma_T n_2 t)}{\sigma_T n_2 t}\right] . \tag{25}$$

In Eq. (24), Y is the summed yield per projectile of projectile and target K vacancies. In Eq. (25), $\sigma_{mc}(2p\sigma, \text{thick})$ is given by Eqs. (17) or (22), $n^{eq}(v_1)$ is given by Eq. (21), $n^b(v_1)$ is the projectile $2p$-vacancy number emerging from the backing foil of atomic density n_b [compare Eq. (D1)][45,57]

$$n^b(v_1) = n^{b,eq}(v_1)[1-\exp(-\sigma_T^b n_b b)] , \tag{26}$$

where $n^{b,eq}(v_1)$ is given by Eq. (21) applied to the backing foil, and σ_T (and, similarly, σ_T^b) is given by

$$\sigma_T = \sigma^p + \sigma^c + (n_2 v_1 \tau)^{-1} . \tag{27}$$

In Eq. (27), σ^p is the projectile $2p$-*vacancy* production cross section in the target foil [of which $\sigma_{proj\,x}^{2p}$, introduced in Eq. (20), is the radiative part], σ^c is the cross section for projectile $2p$-vacancy quenching by target-electron capture[58] or other quenching mechanisms[57] and τ^{-1} is the total (radiative plus Auger) decay constant of projectile $2p$ vacancies. If $n^b(v_1) \ll n^{eq}(v_1)$ and $\sigma_T n_2 t \gg 1$, Eq. (25) gives $\sigma_{mc}(2p\sigma, \text{thin}) = \sigma_{mc}(2p\sigma, \text{thick})$, as it should. If $n^b = 0$ and $\sigma_T n_2 t \ll 1$, $\sigma_{mc}(2p\sigma, \text{thin}) = 0$, and $\sigma_K^{sum}(\text{thin})$ gives the single-collision cross section.

We have attempted to use Eqs. (18) and (23) in order to explain apparent discrepancies between cross sections measured with thin foils and with thick foils or thick targets. From Eqs. (18) and (23) we see that there exists a difference between a thick-target and a thin-target sum cross section due to the multiple-collision effect:

$$\begin{aligned}\sigma_K^{sum}(\text{thick}) - \sigma_K^{sum}(\text{thin}) &= \sigma_{mc}(2p\sigma, \text{thick}) - \sigma_{mc}(2p\sigma, \text{thin}) \\ &= \sigma_{mc}(2p\sigma, \text{thick})\left(1-\frac{n^b(v_1)}{n^{eq}(v_1)}\right) \\ &\quad\times\frac{1-\exp(-\sigma_T n_2 t)}{\sigma_T n_2 t} .\end{aligned} \tag{28}$$

Kubo *et al.*[2] used targets 10–20 $\mu g/cm^2$ thick mounted on 40-$\mu g/cm^2$-thick C (these are the thicknesses traversed by the beam). Their Br cross sections are up to a factor $\frac{1}{2}$ smaller than our thick-target cross sections [Figs. 4 and 9(a)] and their Ni+Ni cross sections are up to a factor $\frac{1}{3}$ smaller than those of Refs. 33 and 56. In the latter

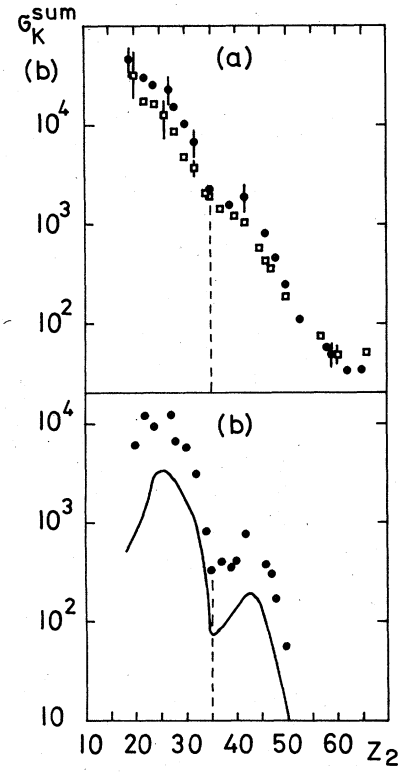

FIG. 9. Comparison of thick- and thin-target cross sections for Br as a function of target Z. (a) Solid symbols, thick target-cross sections from our work; open symbols, thin-target cross sections from Ref. 2. Typical errors (±30%) are shown. Dashed vertical line indicates symmetric collision. (b) Differences between thick- and thin-target cross sections. Data points have errors exceeding cross section differences in most cases, but trend is significant. Curve is expected difference due to multiple-collision effect on $2p\sigma$ cross section [Eq. (28)].

references Ni foils 200 $\mu g/cm^2$ thick were used, which act like thick targets as far as $2p$ multiple-collision effects are concerned.

In applying Eq. (28) one is faced with the difficulty that one can measure only projectile L *x-ray* cross sections but needs to know projectile L *vacancy* cross sections in the solid target. For lack of actual knowledge we assume that the $2p$ fluorescence yield (ω_{2p}^{p}) in the target is equal to twice the value listed in Table IV, XV of Ref. 59 consistent with a lengthening of projectile L-hole lifetimes in solid targets.[60] Also, we find that σ^c in Eq. (27) can be neglected within the uncertain values of capture cross sections.[61,62] Finally, we assume $\tau = \omega_{2p}^{p}\tau_x$, where τ_x is taken from Ref. 48, assuming again that appreciable number of projectile M electrons are present in the solid target.[49]

In Fig. 9(a) we compare our 43-MeV Br sum cross sections with those of Kubo *et al.*[2] for a variety of targets. Although in most cases the differences between the cross sections lie within the experimental errors, there appear to be systematic trends in the differences [Fig. 9(b)], which are reproduced qualitatively by Eq. (28) [curve in Fig. 9(b)]. The curve shown assumes a thickness of 15 $\mu g/cm^2$ for all the targets used in Ref. 2. Minor changes in beam current integration could affect the cross-section differences in a major way, so that the discrepancy in absolute magnitude between the curve and the data points in Fig. 9(b) should not be of major concern.

In Table I we compare thick and thin Ni+Ni cross-section data from Ref. 2 with that of Refs. 33 and 56. We used the $n(v_1)$ values from Ref. 33, shown in Fig. 6(c), to estimate the projectile $2p$ x-ray cross section with the help of Eq. (21). Using $\omega_{2p}^{p} = 0.016$ we deduced the vacancy cross sections needed for Eq. (28). From columns 5, 6, and 7 of Table I we see that Eq. (28) appears to provide a reasonable explanation for the difference between thick- and thin-target cross sections within experimental errors and the other uncertainties.

In summary, the present work demonstrates the importance of multiple-collision effects in solid targets on summed K-vacancy yields. Hence *any* solid-target measurement of the K-vacancy cross section of the *lower-Z* collision partner, and measurements *near symmetry* of the *higher-Z* collision partner must be interpreted with care. One must also be concerned about the influence of multiple-collision effects on the impact-parameter dependence of the K x-ray production probability in the lower-Z partner, if solid targets are used.[63,64] Multiple collision effects in solid targets invalidate the application of scaling laws to solid-target K-vacancy cross sections near symmetry.[39,56,65]

The multiple-collision effects discussed above are not to be confused with the additional effects which occur if appreciable steady-state (residual) K vacancies are present in the projectile.[45,57] In that case capture of target electrons into the projectile K shell can modify the target and the projectile K x-ray yields. The equilibrium fraction of steady-state K vacancies in the projectile can be estimated from a formula similar to Eq. (A18). For 43-MeV Br in KBr the equilibrium fraction of projectile K vacancies is approximately 10^{-5}. Hence in our work the summed target and projectile K cross sections are not affected by K capture effects.

C. Single-collision $2p\sigma$ cross section

For $Z_1, Z_2 \geq 10$ production of $2p\sigma$ vacancies can occur by *one-step* ionization or by a *two-step* process in which an electron in the initially filled $2p\pi$ MO is excited to a vacant state, such as the $3p\pi$ (Fig. 2), and the $2p\pi$ vacancy then couples into the $2p\sigma$ MO later in the collision.[21] It has also been suggested that in a given collision both processes can occur.[66,67] Although one might presume that these processes are coherent, the one-step excitation is largest to final continuum states, similar

TABLE I. Comparison of thick- and thin-target summed Ni+Ni K-vacancy cross sections.[a]

E_1 (MeV)	σ_K^{sum}(thick) (b)	(c)	σ_K^{sum}(thin) (d)	σ_K^{sum}(thick)−σ_K^{sum}(thin) (b)	(c)	Eq. (28)[e]
45	4.0±0.8	2.8	1.3±0.2	2.7±0.8	1.5±0.2	2.1±0.4
61	6.9±1.4	4.4	2.6±0.5	4.3±1.5	1.8±0.5	3.5±0.7
94	•••	8.6	4.5±1.0	•••	4.1±1.0	7.2±1.4

[a] All cross sections in 10^4 b.
[b] Reference 33 (thickness = 200 $\mu g/cm^2$).
[c] Reference 56 (thickness ≃ 200 $\mu g/cm^2$). No errors given.
[d] Reference 2. Assumed target thickness = 15 $\mu g/cm^2$ on 40 $\mu g/cm^2$ C backing, with the backing facing the beam.
[e] Values used for $\sigma_{proj\,x}^{2p}$ at $E_1 = 45$, 61, and 94 MeV are 9, 12, and 18×10^4 b (±20%), respectively.

to $1s\sigma$ ionization,[5] whereas the two-step process should proceed preferentially to the nearest vacant bound states. Hence the two processes should be incoherent and separable.

Experimentally, the single-collision cross section $\sigma_{sc}(2p\sigma)$ can be obtained from gas-target measurements or, in principle, from solid-target measurements, if the multiple-collision contribution is subtracted [Eq. (18) or (23)]. Unfortunately, as shown in Figs. 7 and 8, the multiple collision contribution is very large near symmetry. For reasons given at the end of Sec. II B 2 we are hesitant to rely on the subtraction $\sigma_K^{sum}(2p\sigma) - \sigma_{mc}(2p\sigma)$ for solid targets, even for asymmetric collisions, where the difference is quite large at higher bombarding energies (Fig. 8). Therefore, in this section we use only gas-target cross sections for comparison with various theoretical proposals.

1. One-step process

The only *ab initio* calculation for ionization from the $2p\sigma$ MO has been made for $H^+ + H$ by Thorson and co-workers.[68] As pointed out by them, the ionization really takes place from the $2p\sigma$-$2p\pi$ manifold which is strongly mixed at small internuclear distances.[69,70] Despite this strong mixing, a model calculation has been made, assuming that the role of the $2p\pi$ state is not too important and that the process proceeds mainly by radial and rotational coupling from the $2p\sigma$ state to the continuum.[15]

If screening and nuclear Coulomb repulsion can be neglected, the $H^+ + H$ calculation should scale to higher-Z symmetric systems such that $Z^2\sigma(2p\sigma)$ is a unique function of v_1/Z.[13,15] Foster *et al.*[65] remark that in an actual heavy-ion collision the screening of continuum states is quite different from that in $H^+ + H$ and, therefore, the scaling of $H^+ + H$ ionization calculations to higher-Z symmetric collisions should not be valid. We would like to argue, though, that, by using experimental K binding energies in the scaled $H^+ + H$ calculations, the most important effect of screening is taken into account. Therefore, we take the viewpoint that Z scaling from $H^+ + H$ does provide a sufficiently valid comparison with experiment from which the importance of the $2p\sigma$ ionization process may be judged. In Fig. 10(a) we show such a comparison. Instead of v_1/Z or $(v_1/Z)^2$ we have chosen the velocity scaling parameter to be $[v_1/v_{2p}(U)]^2 \equiv (E_1/M_1)/[I_{2p}(U)/m]$, where $I_{2p}(U)$ is the (united-atom) UA $2p_{1/2}$ binding energy. (The scaling parameter is practically the same as that proposed in Ref. 39.)

Figure 10(a) shows that for $Z = 16$ to 54, this scaling correlates the data above $(v_1/v_{2p})^2 \simeq 2 \times 10^{-2}$ and that at high velocities it connects with the measured ionization cross section for $H^+ + H$, multiplied by 4.[39] The $Ne^0 + Ne^0$ (neutral Ne collsion) cross sections lie considerably above the others, possibly indicating an additional excitation process in this case.

The solid line in Fig. 10(a) is the $H^+ + H$ calculation of Ref. 68, multiplied by four.[39] (This was plotted incorrectly in Refs. 39 and 71.) Since the $1s\sigma$ calculation of Ref. 68 has been shown to have

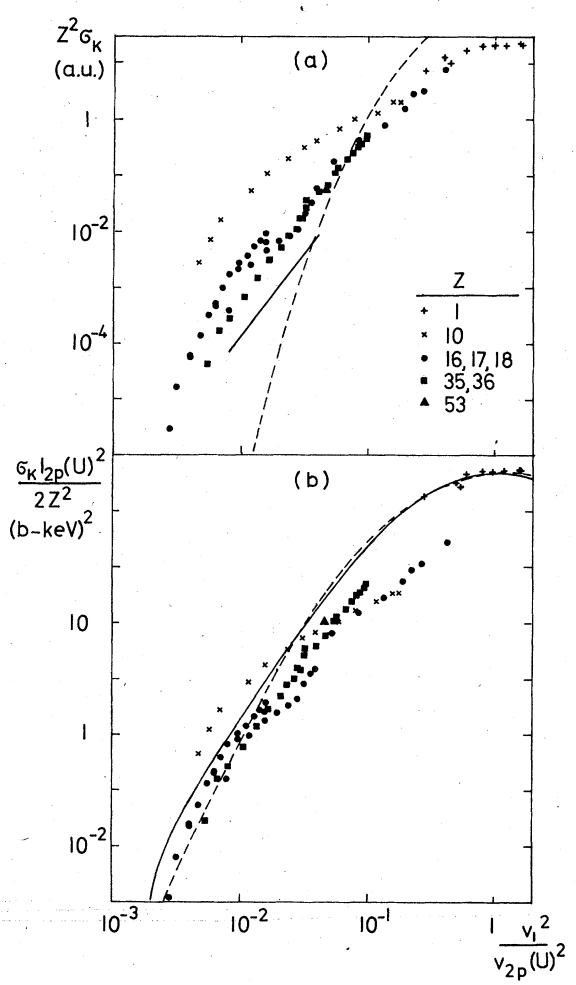

FIG. 10. Scaled summed K-vacancy single-collision cross sections for symmetric collisions. Only gas-target data are used. The cross section and energy scaling parameters are given in the text. All data from Fig. 4, where references are given, except for $H^+ + H$ see Ref. 39. Typical errors lie between ±15% and 30%. (a) Solid line gives scaled $H^+ + H$ $2p\sigma$ ionization cross section from Thorson *et al.* (Ref. 68). Dashed curve is based on proposal by Briggs (Ref. 73). (b) Curves give BEA functions $F(1s)$ (solid curve) and $F(2p)$ (dashed curve) from Hansen (Ref. 8), according to modified-BEA proposal of Ref. 65.

major integration errors,[72] the $2p\sigma$ calculation may also be uncertain. Hence one cannot judge from Fig. 10(a) whether or not experiment is in agreement with the *ab initio* theory, even if screening were properly taken into account. There is the additional uncertainty that the experimental cross sections, except for $H^+ + H$, include transitions to bound MO's, whereas the theory does not. As discussed in Ref. 39, excitation to bound MO's should at most double the cross section.

A different theoretical approach to ionization has been proposed by Briggs.[73] He shows that in the straight-line approximation the ionization probability for a symmetric collision $Z \to Z$ with a projectile velocity v_1 can be related to the SCA probability for the collision $Z \to 2Z$ with a projectile velocity $\frac{1}{2}v_1$. A symmetry restriction allows electron transitions from a given initial bound state only to continuum states of equal parity. Integrating the ionization probability over all impact parameters one then finds for the $2p\sigma$ ionization cross section

$$\sigma(Z \to Z, v_1, 2p\sigma) = 16\sigma_{\mathrm{SCA}}(Z \to 2Z, \tfrac{1}{2}v_1, 2p \to p_{\mathrm{cont}}) . \tag{29}$$

Here we assume that the important SCA ionization amplitudes are those to s, p, and d continuum states,[74] so that in the restricted SCA cross section only transitions from the UA $2p$ to continuum p states must be used.

In Fig. 10(a) the dashed curve is the result of our evaluation of Eq. (29). We have used tabulated SCA cross sections[6] with a typical value of 0.6 for the screening constant θ_L. To correct for the proportion of the cross section going to continuum p states we have used an estimate obtained from Ref. 75 which yields

$$\frac{\sigma_{\mathrm{SCA}}(2p \to p_{\mathrm{cont}})}{\sigma_{\mathrm{SCA}}(2p \to s, p_{\mathrm{cont}})} \simeq \left[1 + 0.0516\left(\frac{v_{2p}}{v_1}\right)^2\right]^{-1} . \tag{30}$$

Reference 75 uses the Huus approximation,[5,6] which is valid only for $v_1/v_{2p} < 0.2$, but this is just the region where the disagreement with experiment is worst.

The discord between the two $2p\sigma$ ionization estimates shown in Fig. 10(a) is severe. Indeed, the work of Ref. 75 indicates that for slow collisions the energy dependence of the $2p \to p_{\mathrm{cont}}$ ionization cross section is E_1^6, whereas Ref. 15 gives approximately E_1^3. In view of this situation it appears premature to draw any conclusion about the relative importance of ionization in $2p\sigma$ vacancy production.

Keeping in mind the preceding remark, we draw attention to a proposal by Hansen[8] and by Foster *et al.*[65] that the binding energy effect on "atomic" ionization cross sections could be simulated by substituting the UA binding energy for the SA binding energy in the BEA.[7,8] This substitution produces the scaling relation shown in Fig. 10(b), in which $\sigma_K^{\mathrm{sum}} I_{2p}(U)^2/2Z^2$ is plotted against $[v_1/v_{2p}(U)]^2$. Foster *et al.* suggest that the scaled cross sections should follow the BEA function $F(1s)$, but we show also the BEA function $F(2p)$, both taken from Ref. 8. Omitting the case of $Ne^0 + Ne^0$, in which an additional process may operate, the function $F(1s)$ overestimates most cross sections by nearly an order of magnitude. The function $F(2p)$ appears to give somewhat better agreement for $[v_1/v_{2p}(U)]^2 \lesssim 10^{-2}$, but the energy dependence of the cross section is not well reproduced at higher energies with either function.

For asymmetric collisions, *ab initio* calculations are not available. We show in Fig. 11(a) comparison of the very sparse gas-target cross-section data with the modified BEA proposal of Ref. 65. Although the Z_2 dependence of the cross sections is well reproduced, the cross sections are again overestimated by large factors. [In this velocity range the BEA function $F(1s)$ and and $F(2p)$ have very similar magnitudes.]

We conclude from Figs. 10 and 11 that the importance of the one-step $2p\sigma$ excitation process cannot be ascertained without further theoretical work.

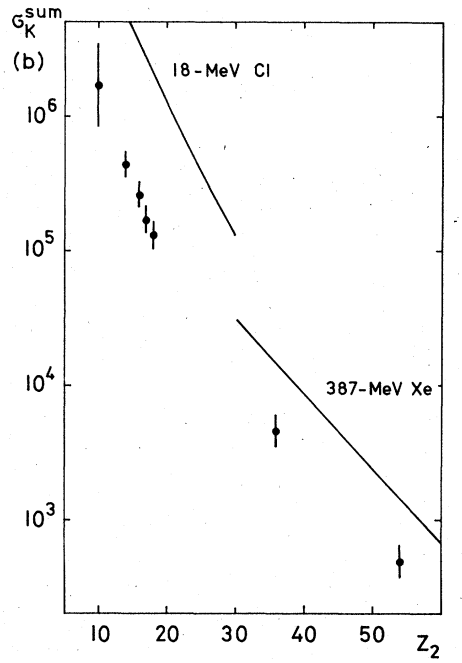

FIG. 11. Summed K-vacancy gas-target cross section for asymmetric collisions as a function of target Z. Data: 18-MeV Cl from Ref. 34, 387-MeV Xe from our work. Curves give modified-BEA proposal of Ref. 65.

2. Two-step process

Since the two-step process of $2p\sigma$ vacancy formation consists of long-range coupling of the $2p\pi$ MO to vacant π MO's, followed by $2p\sigma$-$2p\pi$ electron promotion it has been suggested[21,76] that one might write for this process

$$\sigma(2p\sigma) = N(v_1)\sigma_{\rm rot} \,. \tag{31}$$

Here $\sigma_{\rm rot}$ is the $2p\sigma$-$2p\pi$ rotational-coupling cross section per incident $2p\pi_x$ vacancy[13,42] and $N(v_1)$ is a factor which describes the long-range coupling. Equation (31) has to be modified if $2p$ vacancies are present in the projectile or the target at the beginning of the collision.[21] Empirically one finds that for Z_1, $Z_2 \lesssim 10$,[21,67,76]

$$N(v_1) \simeq Ce^{-\alpha/v_1} \,, \tag{32}$$

where $C \simeq 1$ and α varies strongly with Z. Figure 12(a) shows $\log N(v_1)$ for symmetric-gas cross-section data (Fig. 4) as a function of v_0/v_1, where v_0 is the Bohr velocity for H. One sees that the v_1^{-1} dependence is only approximate.

From a review by Nikitin[23] one can show that the form (32) for $N(v_1)$ is typical for a large class of nonadiabatic transitions with exponential or power-law radial coupling between orbitals separated by a constant energy gap ΔE. If one so identifies $N(v_1)$, one finds that

$$\alpha = \Delta E/\hbar\kappa \,, \tag{33}$$

where κ^{-1} characterizes the range of the interaction. If the form for κ^{-1} proposed by Olson[77] is used, as in Ref. 22, α/v_1 would be given by an expression similar to Eq. (9b), with I_H identified as the $2p(H)$ binding energy (Fig. 2) and I_L as the binding energy of the vacant p state to which the $2p\pi$ MO couples initially.[76]

In the proposed two-step process the $2p\pi$ orbital would be radially coupled to many vacant π orbitals. Hence Cocke *et al.*[78] suggested that one should identify the binding energy of the vacant π orbital or p state as a mean energy, to be determined experimentally through a comparison of Eq. (32) with Eq. (31). Presumably, except in the case of $Ne^0 + Ne^0$, this mean binding energy would be considerably smaller than the $2p(H)$ binding energy, so for purpose of scaling we prefer to neglect it. Hence we set

$$\alpha/v_1 \simeq 2^{1/2}\pi[I_{2p}(H)]^{1/2}/m^{1/2}v_1 \,, \tag{34}$$

where $I_{2p}(H)$ is the $2p_{1/2}$ binding energy of the higher-Z partner. In Fig. 12(b) we plot the logarithm of $\sigma_K^{\rm sum}/\sigma_{\rm rot} \equiv N(v_1)$ versus the parameter (34) for all the symmetric cross-section data shown in Fig. 12(a). The data of Fig. 12(a) indeed coalesce considerably and approximately follow Eq. (32), shown by the dashed line.

Figure 13 gives $\sigma_K^{\rm sum}/\sigma_{\rm rot}$ for asymmetric collisions, as a function of Z_2. Here the parameter (34) is *constant* for $Z_2 < Z_1$. Therefore, even if the parameter is modified by taking into account the mean binding energy of the vacant p state, $N(v_1)$ should be approximately constant for $Z_2 < Z_1$, in

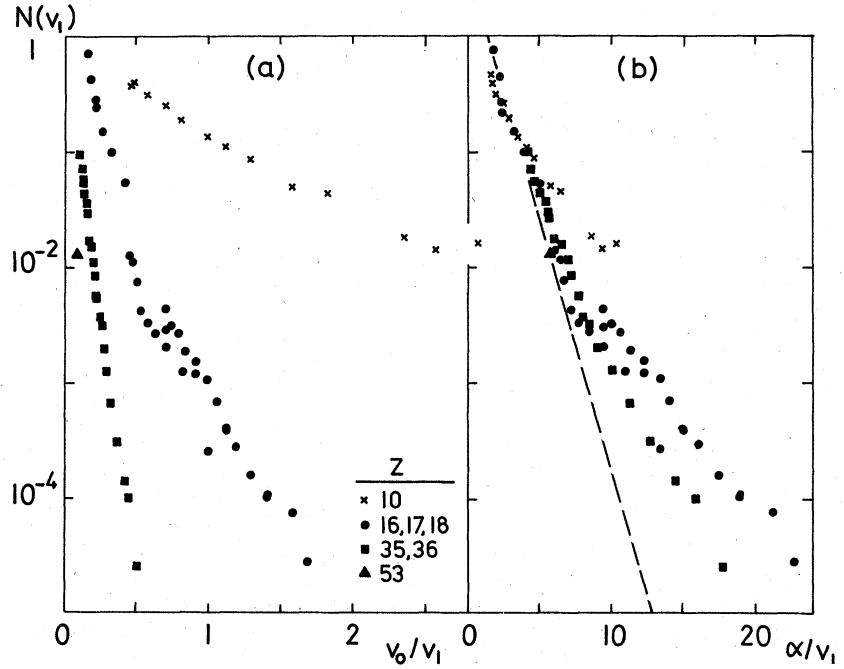

FIG. 12. Single-collision two-step $2p$ vacancy factor $N(v_1)$ for symmetric collisions [Eq. (31)]. The same gas-target data are used, as in Fig. 10. (a) Abscissa is the inverse projectile velocity in a.u. (b) Abscissa is α/v_1, defined in Eq. (34). Line is Eq. (32), arbitrarily normalized.

complete disagreement with the data. Hence we are forced to conclude that the application of Eq. (31) to collisions with $Z_1 \gtrsim 17$ is not valid. This conclusion is contrary to the conclusion of Ref. 78, but leaves open the possibility that in $Ne^0 + Ne^0$ collisions Eq. (32) is applicable.[21] More studies of asymmetric gas-target collisions are needed to settle this question.

III. K-vacancy sharing

According to the present model (Fig. 2) vacancies produced in the $2p\sigma$ MO are shared in the outgoing part of the collision between the higher-Z and lower-Z collision partners, regardless whether the $2p\sigma$ vacancies are produced by single- or multiple-collision processes. Equation (8) shows that the vacancy sharing ratio (9) can be compared directly with the experimental ratio $\sigma(H)/\sigma(L)$ only if the Z_1, Z_2 region is restricted to regions (iii) in Fig. 1, in which neither $1s\sigma$ excitation nor K-L level matching are important. Figure 14 compares the experimental target to projectile K-vacancy ratio with Eq. (9a). For $Z_2 < Z_1$ this ratio is given by $(1-w)/w$, whereas for $Z_2 > Z_1$ the ratio is given by $w/(1-w)$. A simple change of sign of $2x$ in Eq. (9a) allows for both situations. The agreement of Eq. (9) with experiment extends over nearly nine decades and is one of the confirming pieces of evidence for the molecular model of Fig. 2. Very good agreement is also obtained with gas targets.[21,67,79] Therefore, we restrict the subsequent discussion to situations where there is an apparent or real breakdown of Eq. (9).[41,80-82]

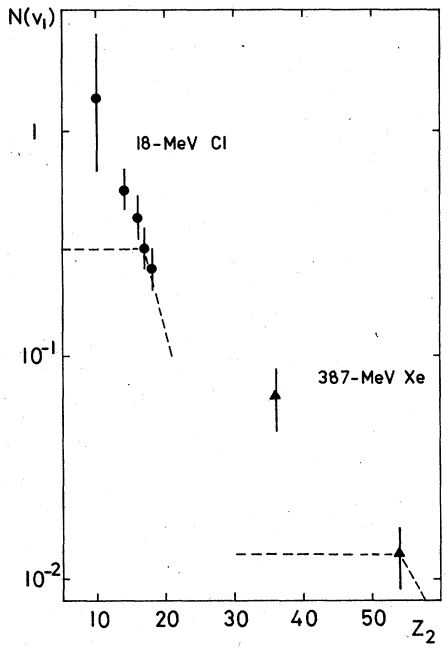

FIG. 13. Single-collision two-step $2p$ vacancy factor $N(v_1)$ for asymmetric collisions [Eq. (31)] as a function of target Z. The same gas-target data as in Fig. 11 are used. According to Eqs. (32) and (34), $N(v_1)$ should be approximately constant below symmetry, as shown.

Jones *et al.*[80] determined $\sigma(H)/\sigma^K_{\rm sum}$ [see Eqs. (2) and (7)] for a variety of targets between Al and Ni, bombarded with 0.75- to 16-MeV Ar. Up to Ti reasonable agreement was found with the vacancy fraction w computed from Eq. (9), but for the higher-Z_2 values and at the lower bombarding energies major deviations were noted. In Fig. 15 we present the Ar+Cr and Ar+Ni results of Ref. 80, with the abscissa $2x$ defined in Eq. (9b). The solid line is the calculated value of w, obtained from Eq. (9a),

$$w = (1+e^{2x})^{-1}. \tag{35}$$

Jones *et al.* attempted to correct their results for target recoil,[25,26] using the formulas of Ref. 83 in an approximate manner. If target recoil and straggling contribute the cross sections σ_R and σ_S, respectively, to the higher-Z vacancy production,

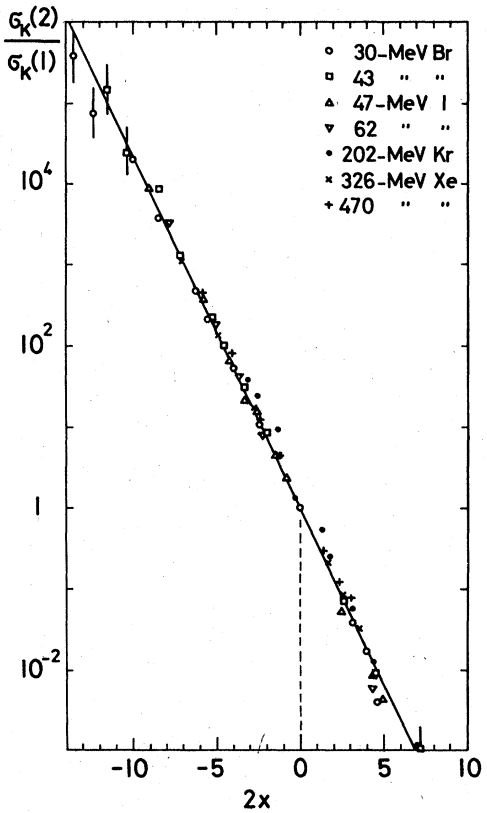

FIG. 14. Target to projectile K-vacancy cross section ratio as a function of K-vacancy sharing parameter $2x$ defined in Eq. (9b). Straight line is Eq. (9a). Dashed vertical line indicates symmetry.

assuming the target to be the higher-Z partner, one finds from Eqs. (4) and (7),

$$\sigma_K(H)/\sigma_K^{\rm sum} \simeq w + [\sigma(1s\sigma) + \sigma_R + \sigma_S]/\sigma(2p\sigma). \quad (36)$$

This equation applies outside the K-L level matching region, which is the case for Ar+Cr, Ni. We estimate the various cross sections in Eq. (36) as follows. For $\sigma(1s\sigma)$ we use the formula of Basbas *et al.*[16] for Z_1+Z_2 encounters with $Z_1 \ll Z_2$, but with a weakened binding-effect correction, as described in Ref. 84 (see also Paper III). For the recoil and straggling cross sections σ_R and σ_S we use Eqs. (B2) and (B1) of Ref. 1, which are based on the thick-target formulas of Ref. 83. We find that $\sigma(1s\sigma)$ and σ_S are negligible compared to σ_R. For $\sigma(2p\sigma)$ we use the prescription of Foster *et al.*[65] discussed in Sec. II C 1, hoping that the overestimate, illustrated in Fig. 11, approximately equals the multiple-collision effect in the solid Cr and Ni targets. The dashed lines in Fig. 15 give the computed values of $\sigma(H)/\sigma_{\rm sum}^K = w + \sigma_R/\sigma(2p\sigma)$. The overall agreement with the experimental values of Jones *et al.*[80] is sufficiently good, that we believe the entire deviation from w to be due to the recoil effect, even though Jones *et al.* attach some significance to the difference between their calculated recoil corrections and experiment. (Their recoil corrections were made in a more approximate manner than ours.)

In connection with Figs. 14 and 15 we note that a theoretical low velocity deviation from Eq. (9) originally found by Taulbjerg and Briggs has been ascribed to a calculational error.[12] So far, then, no significant low-velocity deviation from Eq. (9) has been established up to $|2x| \approx 14$.

A high-velocity deviation is predicted theoretically by Taulbjerg *et al.*[42] Macdonald[82] and we[85] looked for an experimental verification, using the Cl cross-section measurements of Winters *et al.*[34] Here, again, Eq. (8) applies. Recoil and straggling effects are negligible, because gas targets were used exclusively. For $Z_L/Z_H \gtrsim 0.8$, the theory of Ref. 42 gives practically the same prediction as Eq. (9), in agreement with experiment (top of Fig. 16). For $Z_L/Z_H \simeq 0.6$, Ref. 42 predicts the high-velocity (low-x) deviation shown by the dashed line in the lower part of Fig. 16. It is consistent with experiment, but, unfortunately, the experimental results are not precise enough to verify the theory. In view of the results persented in Fig. 14 the low values of $\sigma(H)/\sigma(L)$ in Fig. 16 in the range $4 \le 2x \le 7$ probably are due to inaccuracies in the Ne fluorescence yield.[34] The dash-dot line is an evaluation of Eq. (8) for Cl+Ne collisions for $x > 3$. Here $\sigma_{K\text{-}L} = 0$ and the estimated values of[84] $\sigma(1s\sigma)$ and[65] $\sigma(2p\sigma)$ could be normalized to experiment. Qualitatively, the trend

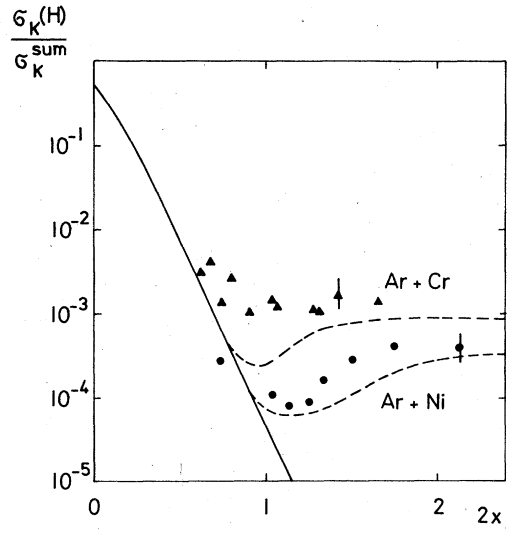

FIG. 15. Fractional K-vacancy cross section of higher-Z collision partner for Ar+Cr and Ar+Ni collisions, as a function of the vacancy sharing parameter $2x$ [Eq. (9b)]. Data from Ref. 80. Solid line gives the theoretical vacancy fraction w defined in Eq. (35), dashed lines include computed corrections due to target recoil [Eq. (36)].

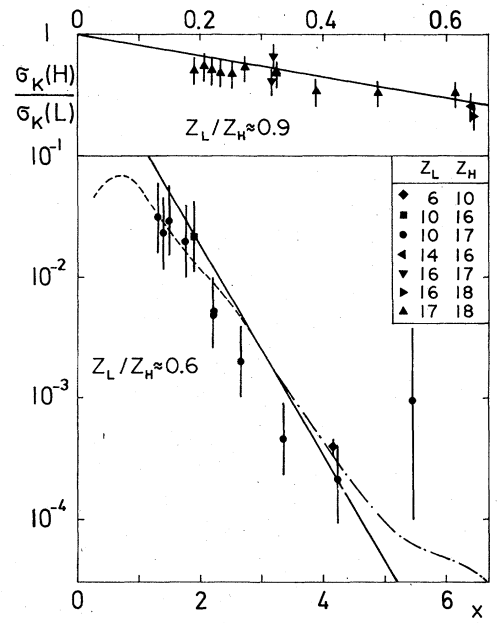

FIG. 16. K-vacancy ratio of higher-Z to lower-Z partner for a variety of collisions as a function of parameter x [see Eq. (9b)]. Note different abscissa scales for top and bottom parts of figure. Data from Ref. 34, except Ne+C point which is from Ref. 93. Top: Data for $Z_L/Z_H \simeq 0.9$. Solid line is Eq. (9a); prediction of Ref. 42 would be identical. Bottom: Data for $Z_L/Z_H \simeq 0.6$. Solid line is Eq. (9a), dashed line is predicted by Ref. 42, dash-dot line is for Cl+Ne and includes contribution from $\sigma(1s\sigma)$ [Eq. (36)].

of the data in Fig. 16 for $x>4$ is in agreement with Eq. (8). A quantitative comparison is not possible, because the available data is not sufficiently precise. We conclude that more work is needed to confirm the predicted high-velocity deviation from Eq. (9a).[86,87]

Finally, we mentioned that for very low Z_1, Z_2 systems, deviations from Eqs. (9a) and (9b) have been reported by Stolterfoht *et al.*[67,81] and by Fastrup *et al.*[21] These are attributed to two-electron effects,[81] but perhaps can also be explained by a dynamic relaxation of electronic binding energies during the collision, without further modification of Eq. (9b).[67,88]

In summary, the K-vacancy sharing concept embodied in Eqs. (2) and (3) has proved to be very useful. Equations (9a) and (9b) for the K-vacancy sharing ratio appear to be valid over a very large domain of E_1, Z_1, and Z_2. *Ab initio* calculations made so far[12,42] cannot explain the large range of validity of Eqs. (9a), and (9b), which, therefore, may be partly fortuitous.[89]

IV. CONCLUSIONS

The model of K-vacancy formation sketched in Fig. 2 and summarized in Eqs. (2) and (3) has been correlated with a wide variety of data. The concept of a cross section for vacancy production in the $2p\sigma$ MO with subsequent sharing of these vacancies between the two collision partners is in accord with experimental findings. In solid targets $2p\sigma$ vacancy formation appears to be dominated by multiple-collision effects. Steady-state projectile $2p$ vacancies are fed into the $2p\pi$ MO with subsequent rotational coupling to the $2p\sigma$ MO [see Eq. (17)]. Even in thin solid targets, this multiple-collision production of $2p\sigma$ vacancies is very important [Eq. (25)]. Therefore, any interpretations of $2p\sigma$ vacancy formation in solid targets, which do not include the consideration of multiple-collision effects, are subject to doubt.

The single-collision cross sections for $2p\sigma$ vacancy formation are most cleanly studied with gas targets. The two proposed mechanisms for single-collision $2p\sigma$ vacancy production, namely, one-step ionization and two-step long-range $2p\pi$ coupling to vacant π orbitals followed by $2p\sigma$-$2p\pi$ promotion at present cannot be established with any certainty. We have presented apparent experimental disagreements with both proposals. More experimental and theoretical work is needed to clarify the situation.

ACKNOWLEDGMENTS

We acknowledge with pleasure the assistance of David Clark in making some of the new cross-section measurements used in this work. Private communications and helpful comments from W. N. Lennard, I. V. Mitchell, B. Crasemann, B. Fastrup, J. D. Garcia, F. Hopkins, R. L. Kauffman, and F. Saris are gratefully acknowledged.

APPENDIX A: ANALYSIS OF THICK TARGET $2p\sigma$ YIELD

1. Derivation

Following the treatment of Garcia[43] we assume that in the solid target projectiles have either zero or one $2p$ vacancy, with relative fractions f_0 and f_1, such that

$$f_0+f_1=1 . \tag{A1}$$

The extension to higher charge fractions is discussed in Sec. II B 1.

The solution of the rate equation for f_1 with no incoming $2p$ vacancies is given by Eq. (7) of Ref. 43:

$$f_1(R)=\exp\left(\int^{R}\Sigma(R')\,dR'\right)\times\int_{R}^{R_0}\Sigma^{p}(R')\exp\left(-\int^{R'}\Sigma(R'')\,dR''\right)dR' . \tag{A2}$$

Here all quantities are expressed in terms of the residual range $R=R_0-x$, instead of the penetration distance x into the thick target. The total range is denoted by R_0. To take into account composite targets, e.g., KBr, we define the inverse mean free path for projectile $2p$ vacancy production:

$$\Sigma^{p}=\sum_i n_i\sigma_i^{p} . \tag{A3}$$

The atomic target density of species i is denoted by n_i and the corresponding projectile $2p$ vacancy production *in the solid target* by σ_i^p. The total inverse mean free path is

$$\Sigma(R)=\Sigma^{p}(R)+\Sigma^{c}(R)+[v_1(R)\tau]^{-1} , \tag{A4}$$

where we generalize the treatment of Ref. 43 to include the possibility of target-electron capture or other vacancy quenching in the projectile.[45,57,90] The corresponding inverse mean free path is

$$\Sigma^{c}=\sum_i n_i\sigma_i^{c} , \tag{A5}$$

where σ_i^c is the capture cross section for projectile $2p$ vacancy quenching by target atoms i. In Eq. (A4), τ^{-1} is the decay constant of projectile $2p$ vacancies due to radiative and Auger decay.

Following Eq. (8) of Ref. 43, the thick-target yield of projectile and target K x rays is given by

the following equations, assuming for sake of definiteness that the projectile is the higher-Z collision partner:

$$Y^p_{Kx}=\sum_i\int n_i[\sigma^i_{sc}(R)+f_1(R)\sigma^i_d(R)]w_i(R)\omega^p_K(R) \times\exp[-\mu^p_K(R_0-R)]\,dR\,, \tag{A6}$$

$$Y^{ti}_{Kx}=\int n_i[\sigma^i_{sc}(R)+f_1(R)\sigma^i_d(R)][1-w_i(R)]\omega^{ti}_K \times\exp[-\mu^{ti}_K(R_0-R)]\,dR\,. \tag{A7}$$

In Eq. (A6), σ^i_{sc} is the single-collision cross section for $2p\sigma$ vacancy production, introduced in Eq. (10). For convenience we define a double-collision cross section $\sigma_d(R)$ per entering projectile $2p$ vacancy. Using Eq. (11) we find

$$\sigma_d(R)=\tfrac{1}{3}w_{2p}\sigma_{rot}\,. \tag{A8}$$

In Eqs. (A6) and (A7), $w_i(R)$ is the K-vacancy sharing ratio evaluated in Eqs. (9a) and (9b) and discussed in Sec. III. Assuming that the target is placed at 45° with respect to the beam, μ^p_K is the absorption coefficient of projectile K x rays in the target material. Equation (A7) is the K x-ray yield for species i in the target and ω^{ti}_K and μ^{ti}_K are defined similarly as for Eq. (A6). In the following we make the simplifying assumptions that one target species i is dominant in producing $2p\sigma$ vacancies, that the K fluorescence yields ω^p_K and ω^{ti}_K vary only negligibly with projectile energy, and that absorption of K x rays in the target can be neglected, which is valid for Z_1, $Z_2\gtrsim 20$. Dropping the subscript i, we then find for the $2p\sigma$ vacancy yield [compare Eq. (7)]:

$$Y\equiv Y^p_{Kx}/\omega^p_K+Y^t_{Kx}/\omega^t_K \tag{A9}$$

$$=\int_0^{R_0}n[\sigma_{sc}(R)+f_1(R)\sigma_d(R)]\,dR\,. \tag{A10}$$

Following Ref. 43 we compute the first and second derivatives of Y with respect to R_0 and finally obtain an expression for $\sigma_{sc}(2p\sigma)$. Noting that $f_1(R)$ is a function of R_0 as well as of R [Eq. (A2)], we find

$$\frac{\partial Y}{\partial R_0}=n[\sigma_{sc}(R_0)+f_1(R_0)\sigma_d(R_0)]+\int_0^{R_0}n\sigma_d(R)\,\frac{\partial f_1}{\partial R_0}\,dR\,, \tag{A11}$$

where

$$\frac{\partial f_1}{\partial R_0}=\Sigma^p(R_0)\exp\left(-\int_R^{R_0}\Sigma(R')\,dR'\right). \tag{A12}$$

Since by our assumption the entering beam contains no $2p$ vacancies, $f_1(R_0)=0$. Substituting Eq. (A12) into (A11) and differentiating once more, one obtains

$$\frac{\partial^2 Y}{\partial R_0^2}=n\,\frac{\partial\sigma_{sc}(R_0)}{\partial R_0}+\Sigma^p(R_0)n\sigma_d(R_0) +\left(\Sigma(R_0)-\frac{\partial\ln\Sigma^p(R_0)}{\partial R_0}\right)\left(n\sigma_{sc}(R_0)-\frac{\partial Y}{\partial R_0}\right), \tag{A13}$$

Except for the presence of σ_{sc}, Eq. (A13) is equivalent to Eq. (11) of Ref. 43. Whereas Garcia[43] was interested to solve for σ_d, we have a model for σ_d, namely, Eq. (A8), and wish to solve for σ_{sc}:

$$\sigma_{sc}(R_0)=\frac{1}{n}\,\frac{\partial Y}{\partial R_0} -\frac{\Sigma^p(R_0)\sigma_d(R_0)+\partial\sigma_{sc}/\partial R_0-n^{-1}\,\partial^2Y/\partial R_0{}^2}{\Sigma(R_0)-\partial\ln\Sigma^p/\partial R_0}\,. \tag{A14}$$

The total range R_0 can be replaced by the bombarding energy E_1 using the transformations[43]

$$\frac{\partial}{\partial R_0}=S(E_1)\,\frac{\partial}{\partial E_1}\,, \tag{A15}$$

$$\frac{\partial^2}{\partial R_0{}^2}=[S(E_1)]^2\,\frac{\partial^2}{\partial E_1{}^2}+S(E_1)\,\frac{dS(E_1)}{dE_1}\,\frac{\partial}{\partial E_1}\,, \tag{A16}$$

where $S(R_0)=S(E_1)\equiv dE_1/dR_0$ is the energy loss of the projectile in the target material. [The second term on the right-hand side of Eq. (A16) is erroneously omitted in Ref. 43.] Hence the first term on the right-hand side of Eq. (A14) is just the Merzbacher-Lewis cross section $\sigma^{sum}_K(ML,v_1)$ for the summed projectile and target K-vacancy production.[5] Below we examine the relative magnitudes of the various terms on the right-hand side of Eq. (A14). We show that in our situation, with less than 1% error, we can rewrite Eq. (A14) as

$$\sigma_{sc}(v_1)=\sigma^{sum}_K(ML,v_1)-\sigma_d(v_1)\Sigma^p(v_1)/\Sigma(v_1)\,. \tag{A17}$$

This is the expression one would obtain immediately if the energy variation of the projectile in the target could be neglected. Indeed, $\Sigma^p(v_1)/\Sigma(v_1)$ is the equilibrium $2p$-vacancy fraction f_1^{eq} of the beam, which can be seen from Eq. (3) of Ref. 44 or by solving Eq. (A2) for $R_0-R\ll R_0$:

$$f_1^{eq}=\Sigma^p(v_1)/\Sigma(v_1)\,. \tag{A18}$$

Also, $f_1^{eq}\sigma_d$ is just the multiple-collision contribution to $2p\sigma$ vacancy formation [see Eqs. (11) and (A8)]. In Appendix B we show that the ratio Σ^p/Σ in Eq. (A17) can be evaluated directly from the projectile $2p$ x-ray cross section.

2. Estimation of magnitudes

It is convenient to use the fact that over limited ranges of bombarding energy E_1, K- and L-

vacancy yields and cross sections are simple power laws of E_1 (see Fig. 4 and Refs. 1, 2, 52, and 54). Writing

$$Y \propto E_1^{\gamma}, \quad \Sigma^p \propto E_1^{\alpha}, \quad \sigma_{sc} \propto E_1^{\beta}; \tag{A19}$$

and using Eqs. (A15) and (A16), Eq. (A14) becomes

$$\sigma_{sc} = \left[\sigma_K^{sum}(ML, v_1)\left(1 + \frac{(\gamma-1)S + E_1\, dS/dE_1}{E_1\Sigma - \alpha S}\right) - \frac{\sigma_d E_1 \Sigma^p}{E_1\Sigma - \alpha S}\right]\left(1 + \frac{\beta S}{E_1\Sigma - \alpha S}\right)^{-1}. \tag{A20}$$

In this notation, the Merzbacher-Lewis cross section is

$$\sigma_K^{sum}(ML, v_1) = (Y/n)(\gamma/E_1)S\,. \tag{A21}$$

We use our measurements for 30-MeV Br+KBr to make estimates of the various terms in Eq. (A20). The Br+Br collisions are dominant in producing K x rays. We find $\sigma_K^{sum}(ML, v_1) \simeq 10^3 b\,(\pm 30\%)$ and $\gamma \simeq 2.0$. From our measurements $\Sigma^p \simeq 1.7 \times 10^5$ cm^{-1} and from Ref. 48 $(v_1\tau)^{-1} \simeq 2.5 \times 10^6$ cm^{-1}, where we have used a $2p$ fluorescence yield $\omega_{2p}^p \simeq 0.02$. Setting $\Sigma^c = 0$ we obtain a lower limit for $E_1\Sigma \simeq 7.5 \times 10^7$ MeV/cm. Using the energy-loss tables of Ref. 91, corrected as suggested in Ref. 92, we find $S \simeq 6 \times 10^4$ MeV/cm and $E_1\, dS/dE_1 \simeq 2 \times 10^4$ MeV/cm. Hence

$$E_1\Sigma \gg S\,, \quad E_1 dS/dE_1\,, \tag{A22}$$

and Eq. (A17) is obtained from Eq. (A20), since all the exponents γ, α, and β are smaller than 10 (see Refs. 52 and 54 and Fig. 9 of I). The inequality (A22) is found for all collision systems examined by us.

APPENDIX B: ANALYSIS OF THICK-TARGET PROJECTILE L X-RAY YIELD

To evaluate the multiple-collision contribution in Eq. (A17) the ratio (A18) must be determined experimentally. We show that this ratio is directly related to the Merzbacher-Lewis value of the projectile $2p$ x-ray production cross section.

By defining a dynamic fluorescence yield[45] to include the possible quenching of projectile $2p$ vacancies as the projectile traverses the target, we could use directly Eq. (15) of Ref. 43. Nevertheless, we prefer to rederive this equation by using the fact that projectiles with single $2p$ vacancies have a mean free path for radiative decay given by $v_1\tau_x$, where τ_x^{-1} is the radiative decay constant for a single $2p$ vacancy [this is called τ_{1x}^{-1} in Eq. (19)]. In Appendix C we examine the influence of Coster-Kronig transitions to and between the projectile L_2 and L_3 subshells. Here we do not distinguish between the two subshells. The extension to projectiles containing multiple $2p$ vacancies is made in Sec. II B 1.

Denoting the projectile thick-target $2p$ x-ray yield per incident projectile by P_x and following as much as possible the notation of Ref. 43 we have instead of Eq. (13) of Ref. 43:

$$P_x = \int_0^{R_0} dR\, f_1(R)[v(R)\tau_x]^{-1} \exp[-\mu_p(R_0 - R)]\,. \tag{B1}$$

Here μ_p is the absorption coefficient for projectile $2p$ x rays in the target material. Contrary to the situation in Appendix A which deals with K x rays, absorption cannot be neglected here. Equation (B1) essentially expresses the fact that whenever a projectile $2p$ vacancy within the residual range R to $R+dR$ decays radiatively, an x ray is emitted. The quantity $(v\tau_x)^{-1}$ is the radiative mean free path. Vacancy quenching enters into $f_1(R)$ [Eq. (A2)], but does not affect the probability $dR/(v_1\tau_x)$ of radiative decay with a distance dR.[45]

Differentiating Eq. (B1) with respect to R_0 we obtain an equation similar to Eq. (14) of Ref. 43,

$$\frac{\partial P_x}{dR_0} = \frac{f_1(R_0)}{v_1\tau_x} + \int_0^{R_0} \frac{\partial f_1}{\partial R_0}\, \frac{\exp[-\mu_p(R_0 - R)]}{v(R)\tau_x}\, dR - \mu_p P_x\,. \tag{B2}$$

Using the condition $f_1(R_0) = 0$ and substituting Eq. (A12) into Eq. (B2), a second differentiation yields

$$\frac{\partial^2 P_x}{\partial R_0} = \frac{\Sigma^p(R_0)}{v_1\tau_x} + \left(\frac{\partial \ln \Sigma^p}{\partial R_0} - \Sigma(R_0) - 2\mu_p\right) P_x'(R_0) + \mu_p^2 P_x(R_0)\,, \tag{B3}$$

where we use the quantity introduced in Ref. 43:

$$P_x' \equiv \partial P_x/\partial R_0 + \mu_x P_x\,. \tag{B4}$$

Equation (B3) is identical to Eq. (15) of Ref. 43, if the inverse mean free path λ in that reference is identified with the total inverse mean free path Σ which includes quenching [Eq. (A4)].

We can now extract from Eq. (B3) the ratio Σ^p/Σ needed in Eq. (A17):

$$\frac{\Sigma^p}{\Sigma} = v_1\tau_x\left[\left(1 + \frac{2\mu_p}{\Sigma} - \frac{1}{\Sigma}\,\frac{\partial \ln \Sigma^p}{\partial R_0}\right) P_x' + \frac{1}{\Sigma}\,\frac{\partial^2 P_x}{\partial R_0^2} - \frac{\mu^2 P_x}{\Sigma}\right]. \tag{B5}$$

Using an evaluation of the various terms similar to that in Appendix A 2, one can show that for $\mu_p \lesssim 5 \times 10^4$ cm^{-1} all the fractions on the right-hand side of Eq. (B5) proportional to Σ^{-1} are less than

1% in our work. Hence, within this accuracy

$$\Sigma^p/\Sigma = v_1\tau_x P'_x(E_1) \tag{B6}$$

$$= v_1\tau_x[S(E_1)\partial P_x/\partial E_1 + \mu_p P_x(E_1)]\,, \tag{B7}$$

where we have used Eqs. (B4) and (A15). The quantity in square brackets, i.e., $P'_x(E_1)$, can be evaluated experimentally from the thick-target projectile $2p$ x-ray yield, independent whether the target is elemental or a compound. This quantity is related directly to the Merzbacher-Lewis cross section[5] for the projectile $2p$ x rays:

$$P'_x(E_1) = \sum_i n_i \sigma^{2p}_{\mathrm{proj}\,x,\,i}(ML, v_1)\,. \tag{B8}$$

For an elemental target of atomic density n, Eqs. (B6), (B8), and (A18) give

$$\sigma^{2p}_{\mathrm{proj}\,x}(ML, v_1) = f_1^{\mathrm{eq}}/(nv_1\tau_x)\,. \tag{B9}$$

The advantage of this equation is that it yields directly f_1^{eq} in terms of an experimental cross section. This bypasses the need to know the various cross sections entering into the ratio Σ^p/Σ. Except for the effect of absorption, Eq. (B9) could have been obtained directly from Eq. (B1) by realizing that the Merzbacher-Lewis cross section is related to the incremental yield ΔP_x when the range (i.e., energy) of the projectile is changed from R_0 to $R_0+\Delta R_0$, where ΔR_0 is large enough to equilibrate the $2p$ vacancy fraction:

$$\Delta P_x \simeq n\sigma^{2p}_{\mathrm{proj}\,x}(ML, v_1)\Delta R_0 \tag{B10}$$

$$\simeq (\partial P_x/\partial R_0)\Delta R_0 \simeq f_1^{\mathrm{eq}}(v_1\tau_x)^{-1}\Delta R_0\,. \tag{B11}$$

APPENDIX C: EFFECT OF COSTER-KRONIG TRANSITIONS

In Appendix A we show that $\sigma_{\mathrm{mc}}(2p\sigma)$ can be related directly to the equilibrium value f_1^{eq} of the projectile $2p$ vacancy fraction, and in Appendix B we show that the latter can be obtained from the experimental Merzbacher-Lewis $2p$ x-ray cross section via Eq. (B9). Here we investigate whether Eq. (B9) is affected by Coster-Kronig transitions between the various projectile L subshells. To simplify the notation and the equations, we consider an elemental target of atomic density n. As in Appendix A and B, we assume that projectiles have either zero or one vacancy in any subshell at a given time, so that

$$f_0 + f^{(1)} + f^{(2)} + f^{(3)} = 1\,, \tag{C1}$$

where f_0 is the fraction of projectiles with zero L vacancies and $f^{(i)}$ is the fraction of projectiles with one vacancy in the subshell L_i. Analogous to Eq. (5) of Ref. 43, the rate equations for the vacancy fractions can be written

$$\partial f^{(1)}/\partial x = n\sigma_1^p(1 - f^{(1)} - f^{(2)} - f^{(3)}) - n\sigma_1^c f^{(1)} - (v\tau_1)^{-1}f^{(1)}\,, \tag{C2}$$

$$\partial f^{(2)}/\partial x = n\sigma_2^p(1 - f^{(1)} - f^{(2)} - f^{(3)}) - n\sigma_2^c f^{(2)} - (v\tau_2)^{-1}f^{(2)} + f_{12}(v\tau_1)^{-1}f^{(1)}\,, \tag{C3}$$

$$\partial f^{(3)}/\partial x = n\sigma_3^p(1 - f^{(1)} - f^{(2)} - f^{(3)}) - n\sigma_3^c f^{(3)} - (v\tau_3)^{-1}f^{(3)} + f_{13}(v\tau_1)^{-1}f^{(1)} + f_{23}(v\tau_2)^{-1}f^{(2)}\,. \tag{C4}$$

Here σ_i^p and σ_i^c denote the production and quenching cross sections, respectively, for subshell L_i, τ_i^{-1} is the radiative plus Auger decay constant for subshell L_i:

$$\tau_i^{-1} = \tau_{xi}^{-1} + \tau_{ai}^{-1}\,, \tag{C5}$$

and f_{ij} is the Coster-Kronig probability[59] of shifting a vacancy from the subshell L_i to the subshell L_j.

Despite the complicated nature of Eqs. (C2)–(C4), the discussion following Eq. (B1) indicates that the projectile $2p$ (L_2 and L_3) x-ray yield is given by

$$P_x = \int_0^{R_0} \{f^{(2)}(v\tau_{x2})^{-1}\exp[-\mu_{p2}(R_0 - R)] + f^{(3)}(v\tau_{x3})^{-1}\exp[-\mu_{p3}(R_0 - R)]\}\,dR\,, \tag{C6}$$

where μ_{p2} and μ_{p3} are the effective absorption coefficients for L_2 and L_3 x rays, respectively. Since the single-vacancy x-ray decay constants for the L_2 and L_3 subshells have very similar magnitudes,[48] we can replace Eq. (C6) by Eq. (B1) if a suitable mean absorption coefficient μ_p is defined, and if we set $f^{(2)}+f^{(3)}$ equal to the $2p$ single-vacancy fraction f_1 used in Eq. (B1). Within these approximations result (B9) is again obtained [see Eqs. (B10) and (B11)].

Coster-Kronig transitions do affect Eq. (A18). Although it is not of interest to us to relate the projectile $2p$ single-vacancy fraction $f_1^{\mathrm{eq}}(2p)$ to the vacancy production and quenching cross sections, for completeness we give the altered equation. It is not difficult to show, by using Eq. (C2) and by adding Eqs. (C3) and (C4), that under equilibrium conditions ($\partial f^{(i)}/\partial x = 0$) the following, approximate, equation is obtained, instead of Eq. (A18):

$$f_1^{\mathrm{eq}}(2p) = [\Sigma^p(2p) + \Delta]/[\Sigma(2p) + \Delta]\,, \tag{C7}$$

where

$$\Delta \equiv \frac{\Sigma^p(2s)}{\Sigma(2s)}[(f_{12}+f_{13})(v_1\tau_1)^{-1} - \Sigma^p(2p)]\,. \tag{C8}$$

In these equations

$$\Sigma^p(2p) \equiv n(\sigma_2^p + \sigma_3^p)\,. \tag{C9}$$

We have assumed $\sigma_2^c \simeq \sigma_3^c$, $\tau_2^{-1} \simeq \tau_3^{-1}$, and set

$$\Sigma(2p) \equiv n(\sigma_2^p + \sigma_3^p) + n\sigma_2^c + (v_1\tau_2)^{-1} \quad \text{(C10)}$$

$$= n(\sigma_2^p + \sigma_3^p) + n\sigma_3^c + (v_1\tau_3)^{-1}, \quad \text{(C11)}$$

$$\Sigma^p(2s) \equiv n\sigma_1^p, \quad \text{(C12)}$$

$$\Sigma(2s) \equiv n\sigma_1^p + n\sigma_1^c + (v_1\tau_1)^{-1}. \quad \text{(C13)}$$

Finally, the assumption $f_{23} \simeq 0$ has been made to obtain Eqs. (C7) and (C8).

APPENDIX D: MULTICOLLISION EFFECTS IN THIN-TARGET YIELDS

We compute the multicollision contribution to the $2p\sigma$ cross section in a thin target which is mounted on a backing foil, such that the beam *first* traverses the backing foil. We neglect the energy change of the beam in the foils.[45,57,60] Assuming that no projectile $2p$ vacancies are present before entering the backing foil, the fraction of the beam carrying $2p$ vacancies upon leaving the backing foil is[45]

$$f_1^b = f_1^{b,\mathrm{eq}}[1 - \exp(-\Sigma^b b)]. \quad \text{(D1)}$$

Here $f_1^{b,\mathrm{eq}}$ is the equilibrium fraction of $2p$ vacancies in the backing foil, defined as in Eq. (A18), Σ^b is given by an equation similar to Eq. (A4), and b is the thickness of the backing foil traversed by the beam. In the cases we have examined, the backing foils are so thick that the $2p$ vacancies have equilibriated: $f_1^b = f_1^{b,\mathrm{eq}}$. From Ref. 45 one can obtain the $2p$ vacancy fraction of the beam at a penetration distance x in the target foil

$$f_1(x) = f_1^{\mathrm{eq}} - (f_1^{\mathrm{eq}} - f_1^b)\exp(-\Sigma x). \quad \text{(D2)}$$

where f_1^{eq} and Σ are given by Eqs. (A18) and (A4), respectively, and refer to the target foil. We stress that in Refs. 45 and 57 this equation has been applied to K x-ray production, whereas we use it for $2p$ vacancies in order to compute $2p\sigma$ vacancy formation. Here, in particular, it is not possible to form $2p\sigma$ vacancies behind the target foil.

We follow Eqs. (A6)–(A8) and use Eq. (A10) to compute the yield of $2p\sigma$ vacancies in the target foil of atomic density n:

$$Y = \int_0^t n[\sigma_{\mathrm{sc}}(x) + f_1(x)\sigma_d(x)]\,dx, \quad \text{(D3)}$$

where t is the thickness of target foil traversed by the beam. Upon substitution of Eq. (D2), Eq. (D3) is readily integrated to give

$$Y/(nt) = \sigma_{\mathrm{sc}} + f_1^{\mathrm{eq}}\sigma_d - (f_1^{\mathrm{eq}} - f_1^b)\sigma_d \times [1 - \exp(-\Sigma t)]/\Sigma t. \quad \text{(D4)}$$

This equation is similar to Eq. (3) of Ref. 60. If no backing foil is present, one sets $f_1^b = 0$.

---

*Supported in part by the NSF.

†Formerly at Lawrence Berkeley Laboratory, Berkeley, Calif., where some of this work was done under support from the U. S. ERDA.

‡Present address: Dept. of Physics, Rutgers University, New Brunswick, N. J.

[1]W. E. Meyerhof, T. K. Saylor, S. M. Lazarus, A. Little, R. Anholt, and L. F. Chase, Jr., Phys. Rev. A 14, 1653 (1976) (Paper I).

[2](a) F. C. Jundt, H. Kubo, and K. H. Purser, in *Proceedings of the International Conference on Inner Shell Ionization Phenomena and Future Applications*, edited by R. W. Fink, S. T. Manson, J. M. Palms, and P. V. Rao (U. S. ERDA, Oak Ridge, 1973), p. 1450; (b) H. Kubo, F. C. Jundt, and K. H. Purser, Phys. Rev. Lett. 31, 674 (1973); (c) F. C. Jundt (private communication).

[3]C. H. Rutledge and R. L. Watson, At. Data Nucl. Data Tables 12, 195 (1973).

[4]F. D. McDaniel and J. L. Duggan, in *Beam Foil Spectroscopy*, edited by I. A. Sellin and D. J. Pegg (Plenum, New York, 1976), p. 519; F. D. McDaniel, T. J. Gray, R. V. Gardner, G. M. Light, J. L. Duggan, H. A. Van Rinsvelt, R. D. Lear, G. H. Pepper, J. W. Nelson, and R. A. Zander, Phys. Rev. A 12, 1271 (1975); R. M. Wheeler, R. P. Chaturvedi, J. L. Duggan, J. Tricomi, and P. D. Miller, *ibid.* 13, 958 (1976); T. J. Gray, P. Richard, R. L. Kauffman, T. C. Holloway, R. K. Gardner, G. M. Light, and J. Guertin, *ibid.* 13, 1344 (1976); J. Tricomi, J. L. Duggan, F. D. McDaniel, P. D. Miller, R. P. Chaturvedi, R. M. Wheeler, J. Lin, K. A. Keunhold, L. A. Rayburn, and S. J. Cippola, *ibid.* 15, 2269 (1977); T. J. Gray, At. Data Nucl. Data Tables (to be published); S. R. Wilson, J. R. Rowe, J. L. Duggan, F. D. McDaniel, in *Scientific and Industrial Applications of Small Accelerators, 4th Conf. 1976*, edited by J. L. Duggan and I. L. Morgan, IEEE Publ. No. 76 CH 1175-9NPS (1976) (available from IEEE Service Center, Piscataway, N. J.), p. 186.

[5]E. Merzbacher and H. W. Lewis, in *Handbuch der Physik*, edited by S. Flügge (Springer-Verlag, Berlin, 1958), Vol. 34, p. 166; G. S. Khandelwal, B. H. Choi, and E. Merzbacher, At. Data 1, 103 (1969); B. H. Choi, E. Merzbacher, and G. S. Khandelwal, *ibid.* 5, 291 (1973).

[6]J. Bang and J. M. Hansteen, Kgl. Dan. Vidensk. Selsk. Mat. Fys. Medd. 31, No. 13 (1959); J. M. Hansteen and O. P. Mosebekk, Nucl. Phys. A 201, 541 (1973); J. M. Hansteen, O. M. Johnsen, and L. Kocbach, At. Data Nucl. Data Tables 15, 305 (1975).

[7]J. D. Garcia, R. J. Fortner, and T. M. Kavanagh, Rev. Mod. Phys. 45, 111 (1973).

[8]J. S. Hansen, Phys. Rev. A 8, 822 (1973).

[9]J. H. McGuire and P. Richard, Phys. Rev. A 8, 1374

(1973); J. H. McGuire, *ibid.* 9, 286 (1974); and At. Data Nucl. Data Tables 13, 491 (1974).
[10]U. Fano and W. Lichten, Phys. Rev. Lett. 14, 627 (1965); W. Lichten, Phys. Rev. 164, 131 (1967).
[11]M. Barat and W. Lichten, Phys. Rev. A 6, 211 (1972).
[12]K. Taulbjerg and J. S. Briggs, J. Phys. B 8, 1895 (1975); J. S. Briggs and K. Taulbjerg, *ibid.* 8, 1909 (1975); Corrigendum, *ibid.* 9, 1641 (1976); J. S. Briggs, Rept. Prog. Phys. 39, 217 (1976); J. S. Briggs and K. Taulbjerg, in *Topics in Modern Physics*, edited by I. Sellin (Springer, Berlin, to be published).
[13]J. S. Briggs and J. H. Macek, J. Phys. B 6, 982 (1973).
[14]J. H. Macek and J. S. Briggs, J. Phys. B 6, 841 (1973).
[15]W. R. Thorson, Phys. Rev. A 12, 1365 (1975), and earlier references given therein.
[16]G. Basbas, W. Brandt, and R. Laubert, Phys. Rev. A 7, 983 (1973); G. Basbas, W. Brandt, and R. H. Ritchie, *ibid.* 7, 1971 (1973).
[17]R. Anholt and W. E. Meyerhof, following paper, Phys. Rev. A 16, 190 (1977) (Paper III).
[18]D. H. Madison and E. Merzbacher, in *Atomic Inner-Shell Processes*, edited by B. Crasemann (Academic, New York, 1975), Vol. I, p. 1.
[19]W. Brandt, in Ref. 2(a), p. 948.
[20]Q. C. Kessel and B. Fastrup, Case Stud. At. Phys. 3, 137 (1973).
[21]B. Fastrup, in *The Physics of Electronic and Atomic Collisions*, edited by J. S. Risley and R. Geballe (University of Washington, Seattle, 1975), p. 361.
[22]W. E. Meyerhof, Phys. Rev. Lett. 31, 1341 (1973). The result derived there turns out to be a special case of a formula previously derived by Nikitin [Ref. 23, Eq. (26) with $\theta = 90°$].
[23]E. E. Nikitin, in *Advances in Quantum Chemistry*, edited by P.-O. Löwdin (Academic, New York, 1970), Vol. 5, p. 135.
[24]K. Taulbjerg, J. Vaaben, and B. Fastrup, Phys. Rev. A 12, 2325 (1975).
[25]K. Taulbjerg and P. Sigmund, Phys. Rev. A 5, 1285 (1972).
[26]K. Taulbjerg, B. Fastrup, and E. Laegsgaard, Phys. Rev. A 8, 1814 (1973).
[27]P. Gippner, K.-H. Kaun, W. Neubert, F. Stary, and W. Schulze, Joint Institute for Nuclear Research, Dubna, USSR, Publication No. E7-7688 (1974) (unpublished); and Nucl. Phys. A 245, 336 (1975).
[28]W. E. Meyerhof, *Abstracts of Second International Conference on Inner-Shell Ionization Phenomena* (University of Freiburg, Freiburg, Germany, 1976), p. 62, and *Abstracts of Fifth International Conference on Atomic Physics*, edited by R. Marrus, M. H. Prior, and H. A. Shugart (University of California, Berkeley, 1976), p. 64.
[29]F. W. Saris and D. J. Bierman, Phys. Lett. A35, 199 (1971).
[30]R. C. Der, R. J. Fortner, T. M. Kavanagh, and J. D. Garcia, Phys. Rev. Lett. 27, 1631 (1971).
[31]H. O. Lutz, J. Stein, S. Datz, and C. D. Moak, Phys. Rev. Lett. 28, 8 (1972).
[32]N. Stolterfoht, D. Schneider, D. Burch, B. Aagaard, E. Bøving, and B. Fastrup, Phys. Rev. A 12, 1313 (1975).
[33]R. Laubert, H. Haselton, J. R. Mowat, R. S. Peterson, and I. A. Sellin, Phys. Rev. A 11, 135 (1975).
[34]L. Winters, M. D. Brown, L. D. Ellsworth, T. Chiao, E. W. Pettus, and J. R. Macdonald, Phys. Rev. A 11, 174 (1975). We are grateful to J. R. Macdonald for providing estimated Ne and Cl fluorescence yields for this data.
[35]F. W. Saris, C. Foster, A. Langenberg, and J. van Eck, J. Phys. B 7, 1494 (1974).
[36]H. O. Lutz, W. R. McMurray, R. Pretorius, I. J. van Heerden, and R. van Reenen, Southern Universities Nuclear Institute, Pretoria, South Africa, 1974 Progress Report, p. 28 (unpublished).
[37]R. L. Kauffman (private communication).
[38]K.-H. Kaun, W. Frank, and P. Manfrass, *Proceedings of the Second International Conference on Inner Shell Ionization Phenomena*, edited by W. Mehlhorn and R. Brenn (University of Freiburg, Freiburg, Germany, 1976), p. 68.
[39]W. E. Meyerhof, R. Anholt, T. K. Saylor, and P. D. Bond, Phys. Rev. A 11, 1083 (1975).
[40]I. V. Mitchell, W. N. Lennard, J. S. Forster, and F. W. Saris (private communication).
[41]W. N. Lennard and I. V. Mitchell, Nucl. Instrum. Meth. 132, 39 (1976); J. Phys. B 9, L317 (1976); W. N. Lennard, I. V. Mitchell, J. S. Forster, and D. Phillips, J. Phys. B (to be published).
[42]K. Taulbjerg, J. S. Briggs, and J. Vaaben, J. Phys. B 9, 1351 (1976).
[43]J. D. Garcia, Phys. Rev. A 11, 87 (1975).
[44]R. J. Fortner and J. D. Garcia, in *Atomic Collisions in Solids*, edited by S. Datz, B. R. Appleton, and C. D. Moak (Plenum, New York, 1975), Vol. 1, p. 469.
[45]H.-D. Betz, F. Bell, H. Panke, G. Kalkoffen, M. Welz, and D. Evers, Phys. Rev. Lett. 33, 807 (1974); F. Bell and H. D. Betz, J. Phys. B 10, 483 (1977).
[46]H.-D. Betz, Nucl. Instrum. Methods 132, 19 (1976).
[47]F. Hopkins, A. Little, N. Cue, and V. Dutkiewicz, Phys. Rev. Lett. 37, 1100 (1976).
[48]J. H. Scofield, At. Data Nucl. Data Tables 14, 121 (1974).
[49]R. L. Kauffman, K. A. Jamison, T. J. Gray, and P. Richard, Phys. Rev. Lett. 36, 1074 (1976).
[50]R. Anholt, W. E. Meyerhof, and A. Salin (unpublished).
[51]S. Datz, C. D. Moak, B. R. Appleton, M. D. Brown, and T. A. Carlson, in *Electronic and Atomic Collisions*, edited by L. M. Branscomb, H. Ehrhardt, R. Geballe, F. J. de Heer, N. V. Fedorenko, J. Kistemaker, M. Barat, E. E. Nikitin, and A. C. H. Smith (North-Holland, Amsterdam, 1971), p. 409. The preliminary I cross-section data presented in Fig. 2 of this reference was disturbed by target mounting difficulties in the Z_2 region between 30 and 70 and has been omitted from our Fig. 5. [S. Datz (private communication).]
[52]H. J. Stein, H. O. Lutz, P. H. Mokler, and P. Armbruster, Phys. Rev. A 5, 2126 (1972).
[53]H. J. Specht, Z. Phys. 185, 301 (1965); P. Armbruster, P. H. Mokler, and H. J. Stein, in Ref. 2(a), p. 396.
[54]H. W. Schnopper, A. R. Sohval, H. D. Betz, J. P. Del vaille, K. Kalata, K. W. Jones, and H. E. Wegner, in Ref. 2(a), p. 1348.
[55]S. Datz, C. D. Moak, B. R. Appleton, and T. A. Carlson, Phys. Rev. Lett. 27, 363 (1971).
[56]J. S. Greenberg, P. Vincent, and W. Lichten, in *Abstracts of International Conference on the Physics of X-Ray Spectra*, edited by R. D. Deslattes (National

Bureau of Standards, Gaithersburg, Md., 1976), p. 180.
[57]F. Hopkins, Phys. Rev. Lett. 35, 270 (1975); T. J. Gray, P. Richard, K. A. Jamison, J. M. Hall, and R. K. Gardner, Phys. Rev. A 14, 1333 (1976); R. K. Gardner, T. J. Gray, C. Schmiedekamp, K. A. Jamison, and J. M. Hall (unpublished).
[58]H. C. Brinkman and H. A. Kramers, Proc. Acad. Sci. (Amsterdam) 33, 973 (1930); V. S. Nikolaev, Zh. Eksp. Teor. Fiz. 51, 1263 (1966) [Sov. Phys.-JETP 24, 847 (1967)].
[59]W. Bambynek, B. Crasemann, R. W. Fink, H. U. Freund, H. Mark, C. D. Swift, R. E. Price, and V. P. Rao, Rev. Mod. Phys. 44, 716 (1972).
[60]L. C. Feldman, P. J. Silverman, and R. J. Fortner, Nucl. Instrum. Methods 132, 29 (1976).
[61]J. A. Guffey, M.Sc. thesis (Kansas State University, 1974) (unpublished).
[62]A. M. Halpern and J. Law, Phys. Rev. A 12, 1776 (1975).
[63]C. L. Cocke, R. Randall, and B. Curnutte, in *Electronic and Atomic Collisions, Abstracts of VIII ICPEAC*, edited by B. C. Cobic and M. V. Kurepa (Institute of Physics, Belgrade, 1973), Vol. 2, p. 714.
[64]K. W. Jones, H. W. Kraner, and W. Brandt, Phys. Lett. 57A, 33 (1976); B. M. Johnson, K. W. Jones, and D. J. Pisano (unpublished).
[65]C. Foster, T. P. Hoogkamer, P. Worelee, and F. W. Saris, J. Phys. B 9, 1943 (1976).
[66]D. Burch, in *The Physics of Electronic and Atomic Collisions*, edited by B. C. Cobic and M. V. Kurepa (Institute of Physics, Belgrade, 1973), p. 97.
[67]N. Stolterfoht, in *Topics in Modern Physics*, edited by I. A. Sellin (Springer, Verlag, Berlin, to be published).
[68]V. SethuRaman, W. R. Thorson, and C. F. Lebeda, Phys. Rev. A 8, 1316 (1973).
[69]W. R. Thorson and H. Levy II, Phys. Rev. 181, 230 (1969).
[70]An example of the dependence of the $2p\sigma - 2p\pi$ mixing amplitude on time can be found in Figs. 5 and 6 of R. D. Piacentini and A. Salin [J. Phys. B 7, 1666 (1974)] and in Fig. 2 of W. Betz, W. Greiner, M. Gros, B. Müller, and J. Reinhardt (in Ref. 38, p. 79).
[71]W. E. Meyerhof, Phys. Rev. A 10, 1005 (1974).
[72]R. Anholt, Ph.D. thesis (University of California, Berkeley, 1975) (unpublished).
[73]J. S. Briggs, J. Phys. B 8, L485 (1975).
[74]L. Kocbach, University of Bergen, Norway, Scientific Report No. 80 (1976) (unpublished).
[75]R. P. Singhal and Vir Singh, Physica (Utr.) 83C, 200 (1976).
[76]W. E. Meyerhof, *Abstracts of the Second International Conference on Inner-Shell Ionization Phenomena* (University of Freiburg, Freiburg, Germany, 1976), p. 59.
[77]R. E. Olson, Phys. Rev. A 6, 1822 (1972).
[78]R. R. Randall, J. A. Bednar, B. Curnutte, and C. L. Cocke, Phys. Rev. A 13, 204 (1976); C. L. Cocke, R. R. Randall, S. L. Varghese, and B. Curnutte, *ibid.* 14, 2026 (1976).
[79]N. Stolterfoht, P. Ziem, and D. Ridder, J. Phys. B 7, L409 (1974).
[80]K. W. Jones, F. C. Jundt, G. Guillaume, and P. Fintz, Phys. Rev. A 12, 1232 (1975).
[81]N. Stolterfoht and U. Leithäuser, Phys. Rev. Lett. 36, 186 (1976).
[82]J. R. Macdonald, Bull. Am. Phys. Soc. 20, 1449 (1975); and private communication.
[83]W. Brandt and R. Laubert, Phys. Rev. A 11, 1233 (1975).
[84]W. E. Meyerhof and R. Anholt, in Ref. 76, p. 56.
[85]W. E. Meyerhof, Stanford University, Department of Physics, Nuclear Physics Group Progress Report for 1974–1975, p. 202 (unpublished).
[86]C. Woods, R. L. Kauffmann, K. A. Jamison, N. Stolterfoht, and P. Richard, J. Phys. B 8, L61 (1975).
[87]W. N. Lennard and J. V. Mitchell (private communication).
[88]J. Vaaben and B. Fastrup (private communication); E. G. Bøving, J. Phys. B 10, L63 (1977).
[89]J. S. Briggs, Rept. Prog. Phys. 39, 217 (1976).
[90]D. Matthews and R. Fortner, in Ref. 56, p. 183.
[91]L. C. Northcliffe and R. F. Schilling, Nucl. Data Tables 7, 233 (1970).
[92]D. Ward, J. S. Forster, H. R. Andrews, I. V. Mitchell, G. C. Ball, W. G. Davies, and G. J. Costa, Atomic Energy of Canada Limited, Reports No. AECL-4914 and 5313 (1975) (unpublished).
[93]N. Stolterfoht and D. Schneider (unpublished results, private communication). See also Ref. 67.